

**A validation study of the shallow slope stability model, SHALSTAB,
in forested lands of Northern California**

by

William E. Dietrich

Department of Geology and Geophysics
University of California Berkeley, CA 94720

and

Rafael Real de Asua
John Coyle¹ Bruce Orr
Martin Trso

Stillwater Ecosystem, Watershed & Riverine Sciences
2532 Durant Avenue, Suite 201 Berkeley, CA 94704

17 June 1998

¹ John Coyle & Associates, 334 State Street. Suite 106, Los Altos, CA 94022

Abstract

SHALSTAB is a coupled, steady-state runoff and infinite-slope stability model which can be used to map the relative potential for shallow landsliding across a landscape. The model is based on the assumptions that shallow surface runoff dictates the pore pressure field and that steady state runoff mimics the spatial pattern of soil pore pressures during transient storms. SHALSTAB can be used as a parameter-free model in which the ratio of the effective precipitation to soil transmissivity (q/T) is calculated and used to assign relative landslide hazard: sites with the lowest q/T for instability are expected to be the least stable areas in the landscape. The value of q/T depends on just two variables: (1) drainage area per width of subsurface flow, and (2) local slope, both of which can be easily evaluated using a digital terrain model (DTM). Because the model is parameter-free, it can be easily used in a validation mode, which allows the model to be rejected if its predictions do not match the observed pattern of landsliding. Furthermore, this means that exactly the same model is used on all landscapes, allowing comparisons of relative slope stability among varying landscapes. SHALSTAB is becoming widely used in the Pacific Northwest as a way of using digital elevation data to delineate potential slope stability over large areas.

The results of model testing conducted in the California Coast Ranges of coastal Mendocino and Humboldt counties are reported here. Aerial photographs taken in 1978 and 1996 were used to map the location and size of all observable shallow landslides for seven watersheds ranging in size from 4.8 to 143 km². A total of 844 in-unit failures (i.e., landslides occurring within timber harvesting units that were not associated with roads) and 354 road-related failures were mapped in the total study area of 281.2 km². Landslides ranged in size from 36 to 17,045 m², with a median area being about 500 m². Elevation contours from United States Geological Survey (USGS) 7.5 minute quadrangle maps were digitized and used to create a 10-m grid that provided the digital terrain framework for the model. Mapped landslides were digitized onto this digital surface. For every 10-m grid cell a value of q/T was determined and for each landslide, which typically covered five or more cells, the cell within the landslide with the lowest q/T value was selected to represent the potential instability of the landslide.

To test the model, we developed a procedure for randomly placing landslides of similar size to those that were mapped onto the digital terrain model. We then compared the distribution of modeled landslides with that of the observed landslides. If the model is successful, the observed (mapped) landslides should be much more common in the least stable areas than randomly generated landslides. In addition, the observed density of landslides (number of landslides per unit area) should be greatest for those areas predicted to be least stable. For each of the seven watersheds tested, the results indicated that SHALSTAB successfully met both of these criteria. Comparison of the seven watersheds using the 1978 landslide data also indicated that the number of landslides mapped per unit area of the watershed increased with the proportion of the watershed assigned to the higher instability categories. These results appear to support the use of SHALSTAB as a landscape-scale screening tool for identifying those watersheds with the greatest potential for shallow landsliding.

On average for each of the 7 watersheds, about 46 percent of the observed landslides and 56 percent of the landslide volume occurred in the two lowest slope stability categories (chronically unstable and $\log(q/T) < -3.1$), which represents on average 8% of the drainage area (ranging from 1 to 23% for the seven watersheds). An average for each of the watersheds of about 58 percent of the observed landslides and 72 percent by volume occurred on grid cells with $\log(q/T) < -2.8$, which represents on average 13% of the drainage area (ranging from 3 to 31 percent). Inclusion of the inner gorge area (mapped by California Division of Mines and Geology) with the first two categories as part of the high hazard delineation significantly improved model performance, but includes a larger area of the watershed.

Data from this study were compared with similar results from two study sites near Coos Bay in the Oregon Coast Range. Here all landslides were mapped in the field. Occurrence of landslides was strongly skewed to low $\log(q/T)$ categories and the proportion of the drainage area that would be mapped as high hazard in order to include a specific proportion of all the landslides was slightly higher than that found in the less steep northern California study areas. For one of the study sites, high resolution airborne laser altimetry was available which permitted analysis to be performed on 2-m grids rather than the 10-m grids used in this validation study. Of the 35 mapped landslides, 94 percent fell in the least stable (chronic) SHALSTAB category. Application of airborne laser altimetry technology to slope stability

modeling in forest lands in California should lead to a greatly improved model performance, with two primary management benefits: (1) more accurate prediction of areas susceptible to shallow landsliding (i.e., a greater percentage of observed landslides would occur in the high instability areas), and (2) a smaller proportion of the land area would be assigned to high instability categories.

To date, L-P has been running SHALSTAB with 10-m grid data and has been classifying areas with $\log(q/T)$ of <-3.1 or chronic instability as high hazard areas. The current prescription for high hazard areas is no harvest without review, which requires geotechnical review before any timber harvesting or road construction is allowed. Inner gorge areas are also treated as high hazard. The data clearly support using at least a $\log(q/T)$ of <-3.1 and the chronic sites to determine high hazard areas. This study was designed to test the basic validity of the model, and not to determine the most appropriate threshold to use in defining high hazard areas. Based on our results, raising the high hazard threshold to <-2.8 would significantly increase the number and volume of landslides that occur in the high hazard area but would also increase the area that would be classed as high hazard. A case can not be easily made, however, for moving the threshold to <-2.5 because by this value the model on average is not significantly better than random, and the area that would be placed as high hazard would be as much as 37 percent of the landscape in some watersheds. It is recommended that as part of the geotechnical review of timberland harvesting plans an effort be made to determine whether elevating the threshold to <-2.8 significantly improves detection of highly unstable areas.

Introduction

Shallow landslides are a major source of sediment delivered to streams. Individual landslides may mobilize in the form of a debris flow, and subsequently travel several kilometers downstream, scouring stream channels of all sediment and wood, then depositing it in a large accumulation when the debris flow comes to rest in a low gradient channel. Although shallow landsliding and associated debris flows are an integral part of natural landscape processes, forest management practices can greatly increase the frequency of their occurrence, which can lead to degradation of stream habitat and loss of habitat features through high sediment loading. With expansion of residential development into areas adjacent to lands managed for timber production, there is also an increased chance of forest management actions triggering landslides that pose a risk to human life and property.

As part of landscape-level landuse planning efforts mandated by various recent state and federal regulations, forest managers have been seeking ways to delineate shallow landslide potential on their lands in order to develop management prescriptions that minimize increases in slope instability while sustaining timber harvesting goals. Two basic approaches have been taken to mapping the landslide potential (see Montgomery and Dietrich 1994). One approach involves creating a map of observed shallow landslides based on interpretation of aerial photographs and field inspections, and then using professional judgement and knowledge of local geology and topography to classify the land into landslide hazard categories. The categories can then be used to specify the types of management that can be conducted in these areas. This is the approach taken in most watershed analyses that follow the Washington State Department of Natural Resources methodology for watershed analysis (WFPB 1997). The strength of this approach is that it is based on field investigations, and if the mapper has adequate knowledge of factors influencing landslide processes, reliable interpretations may often be obtained. Its weakness is that landslide maps only reveal where landslides have occurred, not where they are most likely to occur in the future. Hence, the mapper must rely on intuition and experience to estimate the full extent of landslide potential existing in a watershed. This resulting lack of objectivity makes the process very dependent on the mapper's skills and experience. Furthermore, the mapper will be more inclined to create broad categories of land types to avoid the time-consuming and more error-prone process of making detailed interpretations based on inferred local conditions.

The alternative, and one that is advantageous in cases where the management of large parcels of land is under consideration, is to use an automated procedure based on digital topography and computer analysis. This approach has often relied on statistical analysis to seek correlations between landslide occurrence and a wide range of possible variables. While this approach has the advantage of being driven by empirical data, it does not yield results that can be applied more generally over broader landscapes: the correlations must be verified for each new location with the possibility of new variables

being required to establish a useful relationship. To overcome this limitation, Dietrich et al. (1992) formulated a process-based theory and developed a model that ideally, captures the essential processes controlling landsliding, yet remains simple enough that it can be calibrated and validated. Since then, Dietrich and his collaborators have written several papers reporting on the use, testing, and expansion of this model (Dietrich et al. 1993. Montgomery and Dietrich 1994. Dietrich et al. 1995. Montgomery et al. 1998. Dietrich and Montgomery 1998).

In 1995, Louisiana-Pacific Corporation (L-P) began working with a group of scientists (who have since formed Stillwater Sciences) to review all of their northern California timberlands with the goal of establishing Sustained Yield Plans for their holdings as required by the California State Forest Practices Rules. Given the relatively short time period in which they had to complete their planning process, and their desire to use a holistic, mechanistic approach, L-P elected to use a digital terrain-based approach. This approach uses a tree growth, yield and harvest scheduling model for the forest coupled with prescriptive use as delineated by ecological goals and erosion hazards to protect aquatic resources. This evolving model has since become an essential landuse planning tool for L-P.

Part of this modeling effort involved delineating landslide hazard potential using the digital terrain model (DTM) developed by Dietrich and his collaborators and specifying timber practices based on this model assessment. L-P used this process to specify restrictions on the management practices allowed in areas identified by the model as having high landslide hazard potential. The current management prescription for high hazard areas is "no harvest without review," which requires geotechnical review before any timber harvesting or road construction is allowed. Inner gorges are also treated as high hazard areas, but they must be identified in the field during timber harvesting plan preparation because inner gorge maps do not currently exist for most of L-P's ownership and inner gorge features are often missed by the available topographic maps because of limited resolution and accuracy.

The DTM-based landslide model developed by Dietrich et al. was applied throughout L-P's northern California timberlands without calibration or validation because time constraints required immediate application. The value of such a process-based model is that it can still be useful when applied in this manner however, questions can certainly be raised as to whether the model accurately predicts relative landslide hazard across a landscape. In response to such concerns, L-P sponsored a validation analysis for a selection of watersheds within their holdings thought to represent the range of conditions found on their lands. This report documents the results of the validation study, which constitutes the most detailed validation yet attempted in California. A similar effort has recently been completed by Kate Sullivan and Dave Montgomery for Oregon and Washington (personal communication, 1997).

Here, we briefly review the DTM-based landslide model, now referred to as SHALSTAB (a more detailed description of the model can be found in Dietrich and Montgomery [1998]). Then we discuss the procedures used for mapping actual landslides and validating the model, and the overall results. Data are included from parallel model validation studies conducted in Oregon which showed similar results despite different geologic settings and the use of different sources of topographic and landslide data. These data also suggest that substantial improvements in model accuracy may be obtainable with the very high resolution topographic maps that can now be generated using airborne laser altimetry surveys.

SHALSTAB: A shallow landslide slope stability model

A detailed description and analysis of SHALSTAB is available in Dietrich and Montgomery (1998). In essence, SHALSTAB is a coupled, steady-state runoff and infinite-slope stability model. In this model, runoff is assumed to be generated by shallow subsurface flow and saturation overland flow (see Dunne and Leopold, 1978 for a description of these runoff processes), which is perched on the potential failure plane, and driven downslope by a head gradient equivalent to the local surface topography. Because saturated conductivity tends to decline exponentially with depth (e.g., Wilson and Dietrich 1987, Montgomery et al. 1997) and the mechanically weak and dilated colluvial soil is generally more conductive than the underlying weathered bedrock, these assumptions represent reasonable approximations of the runoff process. Steady-state runoff rarely (if ever) occurs, but it is assumed that the topographic pattern of ground saturation predicted by the steady-state model mimics that which would develop in response to large storms. In the infinite slope stability model, cohesion is eliminated as a variable in order to avoid

having to assign values to spatially and temporally varying soil strength. To partially compensate for the elimination of cohesion, the friction angle is set at 45 degrees, which is relatively high.

Coupling the runoff and slope stability models leads to the following expression for the ratio of effective precipitation (q) to the soil transmissivity (T) for slope instability to occur:

$$\frac{q}{T} = \frac{\rho_s}{\rho_w} \left(1 - \frac{\tan \theta}{\tan \Phi} \right) \frac{b \sin \theta}{a}$$

This equation is the SHALSTAB model. Here a is the drainage area that contributes subsurface flow across a hillslope width, b (typically equal to the width of the landslide scar or the size of a grid cell in a digital terrain model), θ is the local gradient of the ground surface (presumed equal to the failure plane surface), $\tan \Phi$ is the angle of internal friction of the soil and ρ_s and ρ_w are the bulk density of the soil and water, respectively. Note that if $\tan \theta > \tan \Phi$, no rainfall is necessary for instability, hence such sites if they have some soil on them are expected to be most prone to instability. The hillslope is predicted to be stable for all slopes in which $\tan \theta \leq (\rho_s - \rho_w / \rho_s) \tan \Phi$. This is because on such low slopes pore pressures in excess of that which can be obtained at full saturation is required for instability to arise. While excessive pore pressures may, in fact, arise due to exfiltration gradients set up by fracture flow in bedrock, (e.g., Wilson and Dietrich 1987, Montgomery et al. 1997), these effects are not accounted for in this model (the subsurface flow is assumed to be parallel to the ground surface). For a given soil transmissivity (here equal to product of saturated conductivity and soil depth), the greater the drainage area, a , that drains across a specific width, b , of hillslope the smaller the effective precipitation needed for instability. Hence, any place of convergent topography, i.e., a ravine, hollow swale, unchanneled valley, etc., requires less precipitation for instability to arise than do planar hillslopes with the same gradient. The steeper the slope, the less water required for instability and as the gradient of the hillslope approaches the angle of internal friction, the amount of precipitation for instability rapidly declines.

If soil bulk density, friction angle, and soil transmissivity are assumed to be spatially constant and the same in all applications, then the model can be easily applied in a wide range of situations. No tuning of parameters is necessary or even possible, hence the model can be more readily tested (i.e., rejected or accepted [validated] as the case may be). This contrasts with the use of parameter-rich models that are merely modified or calibrated to fit the data and are therefore never rejected. Based on previous work (e.g., Montgomery and Dietrich 1994, Dietrich and Montgomery 1998), a value of 45 degrees was assigned as the angle of internal friction (Φ) and 1.67 as the bulk density ratio value.

Dietrich and Montgomery (1998) describe in detail how digital elevation data can be used to solve equation (1) for individual grid cells across a landscape. For each grid point, the local contribution area to the cell (a), the cell width (b), and the local hillslope angle (θ) are calculated. It then becomes possible to calculate the right hand side of equation (1) and to map the spatial pattern of q/T . The ratio of q/T is small because the transmissivity is always much larger than the effective precipitation. For ease of communication, the logarithm of q/T is used and data are plotted in 0.3 $\log (q/T)$ intervals, which are equivalent to intervals in which precipitation changes by a factor of 2 (**Table 1** provides conversions). Transmissivity may range from about 65 m^2/day in forest soils of low bulk density in Oregon to about 17 m^2/day in denser soils, such as those found in California (Montgomery and Dietrich 1994). As **Table 1** shows, as $\log (q/T)$ increases, the steady-state precipitation rate required to produce instability grows to values unlikely to occur in nature. Hence, if the topography requires values of $\log (q/T)$ of -2.2 or larger, hillslopes are unlikely to fail because of the improbable intensity of rainfall that would be required to initiate instability.

Table 1. Comparison of q/T and $\log(q/T)$ values and the precipitation rate required to initiate instability for soils with relatively high ($T = 65 \text{ m}^2/\text{d}$) and low ($T = 17 \text{ m}^2/\text{d}$) transmissivity.

$q/T(1/\text{m})$	$\log(q/T) (1/\text{m})$	Precip for $T = 65\text{m}^2/\text{d}$ (mm/d)	Precip for $T=17 \text{ m}^2/\text{d}$ (mm/d)
0.00079	-3.1	52	14
0.00158	-2.8	103	27
0.00316	-2.5	206	54
0.00633	-2.2	410	103
0.01266	-1.9	818	214

If $\tan\theta$ equals or exceeds $\tan \Phi$, slope instability will occur even under dry conditions according to the model. We call this category of instability "chronic". One of the hypotheses tested in this validation is that chronic areas should exhibit the greatest slope instability (i.e., the greatest number or volume of landslides per unit area should occur in areas classified as chronic). If $\tan\theta \leq \tan \Phi (1 - \rho_w / \rho_s)$, then slope instability is unlikely as the ground is not expected to fail even at saturation. Grid cells falling into this category are ranked as "stable".

Site selection and landslide mapping procedure

Figure 1 shows the location of the 7 watersheds used for this validation study. Because of their small size and close proximity, Juan and Howard watersheds were combined into one test case referred to as "Rockport". **Table 2** summarizes the areas covered and number of mapped landslides used to test the model predictions. The Noyo, Caspar, and James sites are characterized by broad valley bottoms and modest rates of uplift that are representative of coastal Mendocino watersheds. The 1978 and 1996 coverages of the Noyo site both had sufficient data to allow them to be analyzed separately. There were two different mapping areas analyzed for the Caspar Creek basin, a smaller area (4.8 km^2) mapped by Tom Spittler (1995) from 1992 aerial photographs and extensive field work, and another larger area (21.7 km^2) mapped by John Coyle solely from 1996 aerial photographs (who mapped landslides in all of the other basins for the purposes of this study). The area mapped by Coyle includes the areas previously mapped by Spittler. The Rockport basins are short, steep watersheds which drain directly to the sea. Maple and McDonald watersheds are characteristic of the types found in L-P's landholdings in Humboldt County. All watersheds in this study are underlain by marine rocks, primarily sandstones with varying degrees of tectonic deformation. As revealed by aerial photographic mapping, shallow landslides are common in the study area, although they are often difficult to see from the air where clear-cutting has not occurred. A total of 844 shallow in-unit landslides and 354 road-related landslides were analyzed separately (177 additional road-related failures were noted but not mapped because of time constraints and an initial focus on in-unit failures). The total area covered in this study was 281.2 km^2 .

Table 2: Summary of observations at validation sites

WATERSHED	DRAINAGE AREA (km ²)	NUMBER OF IN-UNIT LANDSLIDES	NUMBER OF ROAD-RELATED LANDSLIDES	INNER GORGE INCLUDED
Caspar (Spittler) (field checked 1992)	4.8	29	14	yes
Caspar (Coyle) (1978 and 1996)*	21.7	103	none mapped (115 total count)	yes
James (1978 and 1996)	18	72	15 mapped (117 total count)	yes
Noyo(1978)	143	207	42	no
Noyo(1996)	143	222	56	no
Rockport (Juan and Howard) (1978 and 1996)	34	148 144 from aerial photographs, 4 from 1997 field surveys None observed in 1996	214	no
Maple (1978 and 1996)	49.9	41 +2 (field 1997)	not counted	no
McDonald (1978 and 1996)	14.6	15+3 (field 1997)	not counted	no

* The dates for each site refer to the date of the aerial photograph used. In each case, the 1978 photographs were black and white and the 1996 were color.

Landslide mapping by J. Coyle followed procedures similar to that suggested by Washington Forest Practices Board (1997). For each watershed, aerial photographs taken in 1978 (black and white; 1:15,280) and 1996 (color; 1:12,000) were used. Observed landslide features were delineated on GIS-produced acetate topographic base maps (which could be overlaid on aerial photographs to help delineate landslides more accurately), and then digitized by hand. Landslide scars can be complex features that are difficult to interpret from aerial photographs and it is difficult to locate them precisely on topographic maps which are often inaccurate. For some areas, the difference between the topography as seen in the aerial photograph and as indicated on the topographic map was tabulated, because the smaller-scale landscape features affecting the location of landslide scars are often not portrayed on the topographic maps. Shallow landslides typically mobilize as debris flows, creating a scour track leading to the channel network. SHALSTAB predicts instability at the site of landslide initiation; therefore, it is preferable to map only the head scar. This was not consistently done however for this mapping effort: hence, average landslide size is overestimated. An attempt was made to estimate whether each scar was formed by a shallow landslide or whether it was the surface expression of a deeper feature (i.e., one involving the underlying bedrock). All deep-seated features were excluded from this analysis.

The success of the SHALSTAB model depends strongly on the quality of the topographic data and on the assumptions regarding controls on runoff and stability being approximately correct. As a check on the model, J, Coyle and C. Surfleet visited approximately 50 landslides and gathered data on location, local slope, soil depth, landslide size and topographic setting. Because drainage area to the slide scars was not measured, and there was considerable uncertainty about exact slide location (relative to that mapped from aerial photographs), and about the appropriate value for the slope of the landslide, a quantitative comparison between predicted and observed q/T values could not be done for most sites visited. Nonetheless, the field check provided important data on landslide size and volume, and helped identify some errors in earlier runs of the SHALSTAB model.

Landslide mapping from aerial photographs will miss small slides and those that occur under dense forest canopy. Although the resulting underestimate of landslide density may be relatively large, the

slides that are observable and mappable can still provide an adequate test of SHALSTAB. In the years following a landslide, revegetation will tend to obscure the slide's scar making it difficult to detect on aerial photographs. The number of landslides detected will therefore depend on the timing of the photography relative to the time of landsliding. Local land use history and storms will also affect landslide damage and detectability. The 1978 aerial photographs document the consequences of the intensive forest management occurring during the 1970's as well as the effects of the March 29, 1974 storm, which resulted in extensive landsliding and the highest discharge of record in Noyo and Caspar creeks. Documentation of the total number of landslides in a watershed that is derived solely from aerial photographs is therefore rarely completely accurate. Nonetheless, the subset of landslides that are mapped can still be used to validate the model.

SHALSTAB Validation Procedure

For each study site, mylar separations of elevation contours and blueline streams from available USGS 7.5-minute topographic maps were scanned and digitized, proofed, and then converted into a 10-m grid format using the TOPOGRID⁰ function of the ARC/INFO⁰ program. This approach has the advantage that it can use the digitized location of stream channels to ensure that the modeled topography near channels more closely matches actual topography. Methods used to calculate q/T in equation (1) for each grid cell are described in detail in Dietrich and Montgomery (1998).

Each map of q/T values was checked for problems that may have arisen from model implementation. During one of these inspections we noticed a systematic error in the results and discovered that a programmer had inadvertently altered the original code (by misplacing one parenthesis). This unfortunate error affected all model runs conducted between mid-1995 and April 1996; consequently, none of the maps produced during this period are accurate. Subsequent correction of the code and rerunning of the model resulted in a much stronger grouping of high hazard areas. This was the first finding of our validation study! The results described below are all based on the corrected model.

In order to compare the model results and documented landslide locations, each digitized polygon representing a landslide scar was overlaid on the grid and any grid cell touched by the scar was counted as part of the landslide. Scars classified as shallow landslide features ranged in size from 36 to 17,045 m². Table 3 summarizes the GIS-calculated dimensions of the mapped landslides. For smaller scars, the overlay method tended to enlarge the size of the scars because the grid's minimum resolution was ten meters and if any part of the polygon touched a grid cell, that cell was included as part of the landslide's area.

Table 3. Median size of shallow landslides in each study watershed.

Watershed	Landslide Area	
	median (m ²)	Mean (m ²)
Caspar-Spittler	696	904
Caspar-Coyle	235	300
James	252	447
Noyo	559	803
Rockport	518	1,038
Maple	235	520
McDonald	405	595

Nearly all the scars touched more than one grid cell, hence a q/T value that represented the site stability had to be selected. We reasoned that the cell with lowest q/T value within the landslide polygon would represent the least stable site and therefore control the site stability; it also seemed reasonable to assume that the digital elevation data tended to underestimate local slope and degree of convergence (a/b). Hence, selecting the lowest q/T may come closest to the actual value at instability. The log of the

q/T values was calculated and each landslide was assigned (based on its minimum log (q/T) value) to one of the categories shown in Table 4.

Table 4. Definition of log (q/T) intervals and instability categories used in the analysis.

log (q/T) interval	Instability Category
hillslope angle = \geq 45 degrees	Chronic
< -3.1	-3.1
$-3.1 \leq$ and < -2.8	-2.8
$-2.8 \leq$ and < -2.5	-2.5
$-2.5 \leq$ and < -2.2	-2.2
$-2.2 \leq$ and < -1.9	-1.9
≥ -1.9	> -1.9
hillslope angle < 21.9 degrees	Stable

The total area of each watershed falling into each of these log (q/T) intervals was also calculated. In two watersheds (Caspar and James) inner gorge areas as delineated by California Division of Mines and Geology maps were treated as a separate category and the number of landslides falling into these inner gorge areas and the total area represented by inner gorges were noted.

Model success was judged in two ways. First, if the value of q/T is to be used as a relative hazard rating, then the mapped landslides should cluster in those areas with the lowest q/T values (i.e., the largest negative log (q/T) values, see **Table 1**). Because we used the minimum q/T value to represent relative instability hazard for each landslide, however, a bias in the results was created. Even randomly located landslides would tend to be concentrated in areas having the lowest q/T values because for each randomly located landslide the lowest q/T value would be chosen to represent the site instability category. Therefore, as a second test, we needed to see if the model would perform significantly better than a random model. To answer this question we developed a random landslide generation model (the random placement model) to compare with the statistics of the actual mapped landslides. Groups of grid cells of approximately the same size as the median landslide size in each watershed were randomly placed throughout each watershed until the number of landslides equaled the number that had been observed. As was done for the observed landslides, the cell with the minimum q/T, value was selected to represent the value for each landslide generated by the random model. This process was repeated an average of 10 times for each site and the median and standard deviation of the number of landslides found in each log (q/T) category listed in **Table 4** was determined. A comparison was then made between observed and randomly generated landslide scars for each watershed to ensure that any apparent success of the model would not be due solely to bias created by the selection of minimum q/T values. If this bias was large and the model did not perform significantly better than the random model, there would be no observable difference between q/T values for the populations of observed landslides versus the randomly generated landslides. This is a stringent test of the model's results which ensured that we did not draw spurious conclusions about model performance.

Results

Figure 2 shows the results from the Noyo watershed for the 1996 landslides to illustrate the analysis performed on each watershed (see the Appendix for corresponding plots of all remaining sites). Maps of $\log(q/T)$ values and landslide locations for each watershed are provided in the appendix. For each site, the number of cells in each $\log(q/T)$ category was determined and the resulting cumulative frequency (or percent area) of the total watershed area falling into each successive category is shown in **Figure 2a** (see curve labeled "area"). This curve shows the predicted potential slope instability across the entire watershed. For the Noyo basin, only about 50 percent of the watershed area is potentially unstable—the remaining lands are characterized by gradients too low to fail even when saturated (i.e., are classified as "stable"). A classification of "chronic" denotes that the cell is sufficiently steep to be potentially unstable even without the addition of water from precipitation. The curve generated by random placement of landslides differs from the total watershed area curve because of the bias that results from selecting only the minimum q/T value in each cluster of cells randomly placed on the landscape. This difference is large: 26 percent of the total watershed area has an assigned instability value of < -2.5 for $\log(q/T)$, whereas about 51 percent of the randomly placed landslides were assigned $\log(q/T)$ values of < -2.5 . The curve for the minimum q/T value for each observed landslide is labeled as "landslides" in **Figure 2a** and is distinctly different from both the total watershed area curve and the random model curve. The difference largely results from the much greater incidence of observed landslides assigned to the chronic and -3.1 categories. By $\log(q/T)$ of -3.1 , 59 percent of the observed landslides have been counted, whereas only 26 percent of the random slides and 11 percent of the total watershed area has smaller q/T values. This is clear evidence that SHALSTAB is successfully predicting areas with greater probability of failure.

Figure 2b and **2c** show landslide density as a function of slope instability category for in-unit and the road-related failures using the Noyo 1996 landslide data. Landslide density is the number of landslides found in a given $\log(q/T)$ interval divided by the total area (km^2) of the watershed included in that category. The density is plotted as a function of the larger bound of that category (e.g., density for the category -3.1 to -2.8 is plotted as a function of -2.8). If the model is not successful at identifying unstable areas (and if there were no bias due to selection of minimum q/T value for each slide), then landslide density should be the same for all instability categories. Because of the bias resulting from using the minimum q/T values, the random landslide density shows a progressively greater concentration of landslides in areas of the highest instability ratings. The curve for observed landslide densities, however, is much different. For $\log(q/T)$ values of < -2.8 , the incidence of landsliding was much higher than that estimated from the random placement model. For areas mapped as "chronic" or those falling into the category of < -3.1 ($\log(q/T)$), the incidence of landsliding is high, equivalent to 9 and 7 landslides per km^2 respectively, for the period recorded by the Noyo 1996 aerial photographs. The large difference in landslide density at low q/T values between the mapped and random placement model demonstrates that SHALSTAB is successful at identifying the most unstable areas of the landscape and that this finding holds true for both in-unit and road-related shallow landslides.

Figures 3 through 8 and **Table 5** summarize SHALSTAB model performance (plots similar to **Figure 2** for individual watersheds are included in the appendix). In each watershed, modeled landslide density was greatest in the most unstable categories and differed substantially from that determined by the random placement model. **Figure 3** shows landslide density for observed and randomly placed landslides for each watershed. Landslide density was very high (up to nearly 150 landslides per km^2) for areas assigned to categories of highest instability. Observed landslide density was greater than that for randomly placed landslides for $\log(q/T)$ values < -2.5 for Caspar (Coyle and Spittler). Observed landslide density was also greater than random for values < -3.1 for Noyo (1978 and 1996), McDonald (1978 and 1996 combined), Rockport (1978 and 1996 combined) and James. In the Maple watershed, only the landslide density in areas within the chronic category differed from random; however, 23 percent of all landslides occurred in lands of this category.

Table 5a. Summary of model results.

Watershed	Cumulative percentage of mapped landslides (in unit) in modeled slope stability category (log q/T)			
	Inner Gorge	-3.1**	-2.8	-2.5
Caspar (Spinier)	69 (20%)* --- n.a.	76 (21%) --- 28 (3%)	86 (23%) --- 48 (7%)	97 (30%) --- 79 (16%)#
Caspar (Coyle)	42 (20%) --- n.a.	45 (22%) --- 19 (3%)	59 (24%) --- 42 (7%)	75 (30%) --- 65 (17%)
James	35 (12%) --- n.a.	63 (17%) --- 43 (7%)	68 (23%) --- 53 (14%)	79 (36%) --- 69 (29%)
Noyo(1978)	n.a.	6Q(11%)	76 (16%)	92 (26%)
Noyo(1996)	n.a.	59 (11%)	68 (16%)	81 (26%)
Rockport	n.a.	85 (23%)	89 (31%)	98 (46%)
Maple	n.a.	26 (1%)	35 (3%)	40 (6%)
McDonald	n.a.	58 (6%)	67 (12%)	83 (21%)

* percentages refer to cumulative percent of area in this slope stability category.

** cumulative percent includes the chronic category

bold numbers represent the area that would be mapped as high hazard to have roughly two-thirds of the landslides occur in it

Table 5b. Summary of model results (for volume).

Watershed	Cumulative percentage of volume of mapped landslides (in unit) in modeled slope stability category (log q/T)		
	-3.1**	-2.8	-2.5
Caspar (Spittler)	50 (3%)*	58 (7%) #	77 (16%)
Caspar (Coyle)	21 (3%)	45 (7%)	71 (17%)
James	53 (7%)	69 (14%)	84 (29%)
Noyo 1978	79 (11%)	85 (16%)	96 (26%)
Noyo1996	68 (11%)	77 (16%)	88 (26%)
Rockport	89 (23%)	91 (31%)	99 (46%)
Maple	35 (1%)	75 (3%)	77 (6%)
McDonald	72 (6%)	82 (12%)	94 (21%)

* percentages refer to cumulative percent of area in this slope stability category.

** cumulative percent includes the chronic category

bold numbers represent the area that would be mapped as high hazard to have roughly two-thirds of the landslide volume occur in it

Figures 4 and 5 show cumulative percentages of landslides found in each log (q/T) category

for in-unit and road-related landslides in the watersheds. Rockport had the greatest proportion of landslides in the lowest $\log(q/T)$ values whereas Maple had over 40 percent of the landslides falling in the stable category. The average cumulative percentage of mapped in-unit landslides in each watershed for the chronic, -3.1, -2.8, and -2.5 categories is 26, 48, 60, and 75 percent, respectively (with a standard deviation of about 21 percent for each category). The numbers are similar for road-related landslides.

Figure 6a shows the cumulative percentage of total area in each landslide instability category for each watershed. The results show that because of its topography alone, the potential for shallow landslide instability is greatest in the Rockport watershed and least in the Maple. While only about 30 percent of the Rockport watershed area is estimated to be stable regardless of storm intensity, over 80 percent is expected to be stable in the Maple watershed. These differences in intrinsic slope instability are reflected in the number of landslides found in each watershed. The total number of landslides in each watershed divided by total drainage area for the 1978 aerial photographs is indicated in **Figure 6a** and **6b**. We selected the 1978 photographs for this comparison because forest management activities were more intense at this time and because the 1974 storm affected many of these basins. Ideally, each watershed would have been subjected to the same timing and intensity of forest harvest activities as well as the same magnitude and duration of storms. Such a similarity was greater for conditions shown in the 1978 than 1996 photographs, but each watershed was subjected to different management actions. Nonetheless, landslide density recorded in the 1978 photographs varied systematically in proportion to the intrinsic instability of the watershed (as reflected the proportion of the watershed sufficiently steep to generate shallow landslides), with the greatest landslide density found in the Rockport and the least in the Maple and McDonald watersheds. This finding lends strong support for the use of SHALSTAB as a tool for regional or landscape-scale classification of watersheds for potential landslide hazard. It should be noted that field observations indicate that where McDonald is sufficiently steep it shows signs of instability including deep-seated landsliding (C. Surfleet, 1998, pers. comm.). McDonald landslide densities are four times higher in 1996 than 1978. The low value in 1978 may be due to particular storm and land use history.

Figure 7 provides a useful summary of the validation test results. For each instability category, the cumulative percentage of landslides found in that category (**Figure 4**) and cumulative percentage of watershed area (**Figure 6**) was calculated. These two attributes were then plotted against each other to reveal how much of the watershed area would have to be categorized as unstable in order to account for a certain percentage of the mapped landslides. For example, to account for 40 percent of all mapped landslides, about 3 to 8 percent of the total watershed area would have to be categorized as unstable. For 60 percent of the landslides to be accounted for, about 7 to 20 percent of the watershed would have to be categorized as unstable. These percentages do not directly correspond to $\log(q/T)$ categories. Note, however, that each data point in **Figure 7** represents a particular instability category, increasing from "chronic" to "stable" as the cumulative percentage of landslides accounted for increases from zero to 100 percent. The bold lines (with labels) represent the average values for the 8 curves. For example, on average for all 8 curves 48 percent of the cumulative percentage of landslides fell into the category of < -3.1 . The percentage of watershed area falling into the chronic or < -3.1 categories ranged from 1 to 23 percent. On average for all 8 curves, 60 percent of the landslides fell in areas with $\log(q/T)$ values less than -2.8; the actual corresponding percentage of total watershed area ranges from 3 to 31 percent. These watershed area numbers are close to the values that would be obtained from reading the intersection of the bold lines with the curves in **Figure 7**, indicating that the selection of a particular $\log(q/T)$ category should give a reasonable estimate of the amount of unstable area within a watershed. The horizontal bold line labeled as chronic indicates the broad range (from 3 to 70 percent) in the percentage of observed landslides accounted for by this category.

This same analysis can be done with the more relevant measure of cumulative landslide volume instead of cumulative landslide number. These numbers differ because in four of the watersheds there is a well defined relationship of decreasing size with increasing $\log(q/T)$ (**Figure 8**). Such a relationship would be expected if the larger landslides are associated with instability in

unchanneled valleys which are typically the least stable elements of the landscape. Landslide area was converted to volume by multiplying by the approximate depth of soil of 1.0-m measured in 28 of the landslide scars visited in the field. **Figure 9a** shows the cumulative percent of landslide volume (compare with **Figure 4**). **Figure 9b** shows the equivalent of **Figure 7** but plotted in terms of volume. The position of the bold lines in **Figure 7** are shown in **Figure 9** as dashed ones, and the new bold lines represent the average cumulative percent of landslide volume for each corresponding $\log(q/T)$ category. In general, for each watershed the model performance is improved, i.e., for the < -3.1 category the percent volume is on average 58 percent (as compared to 48 percent by cumulative number), for < -2.8 it is 73 percent (as compared to 60 percent) and for < -2.5 (it is 86 percent as compared to 76 percent).

Table 5 summarizes model performance. Cumulative percentage of mapped in-unit landslides (by number, Table 5a, and by volume, Table 5b) are shown for each of the lowest q/T categories. Cumulative percentage of watershed area falling into that category is also shown in parentheses. This shows individual variations in the landslide-area relationships that were expressed graphically, in Figures 7 and 9. Table 5 shows (in bold) the cumulative percent watershed area for which the corresponding $\log(q/T)$ category accounts for approximately two-thirds of the number of landslides mapped (Table 5a) or two-thirds of the landslide volume (Table 5b). This cumulative area for percentage of landslide numbers ranged from as little as 6 percent to as high as 21 percent of total watershed area, whereas for landslide volume it ranged from 3 to 23 percent of the watershed area. For Maple, $\log(q/T) < -2.8$ accounted for only 35 percent of the landslides, but 75 percent of the landslide volume.

Table 5a also displays the effect of mapping inner gorge areas as a separate category for three watersheds—Caspar (Coyle and Spittler coverages) and James. Figure 10 illustrates the results. Although a large percentage of the landslides (35 to 69 percent) fell within inner gorge areas, so did a large percentage of total drainage area (12 to 20 percent). Consequently, a greater percentage of the landslides in each watershed (i.e., Caspar-Spittler, Caspar-Coyle, and James) could be associated with a smaller percentage of the landscape area if SHALSTAB alone was used without separate delineation or classification of inner gorge areas using the available CDMG maps. This outcome probably depends on the quality of the topographic map used and how accurately inner gorge areas were delineated on the CDMG maps.

Discussion

Another measure of the validity of this study is to compare it with similar landslide modeling efforts. Figure 11 shows the preliminary results for two areas in the Oregon Coast Range. These are areas of well-developed ridge and valley topography, with maximum local relief of about 300 m, underlain by weakly deformed marine sandstones and shales (see Reneau and Dietrich 1990, 1992) for a more detailed description of the area). Data plotted for Elk Creek were derived from an Oregon Department of Forestry study (Jim Paul, pers. comm.). The 156 landslides included in the Elk Creek study occurred in a 22-km² area in response to an intense storm in November of 1996; all were subsequently mapped in the field. A topographic map was created using aerial photographs, which more accurately portrayed the ridge and valley topography than do available 7.5-minute USGS quadrangles of the area. Because mapping was done in the field and because the topographic map was of a higher resolution, these data should provide a more accurate test of SHALSTAB. The landslides are small here and each landslide was assigned to a single 100 m² grid cell. Figure 12 shows that the landslide density differs greatly from the uniform distribution that a random model would predict. The cumulative percentage drainage area versus cumulative percentage of landslides plotted for Elk Creek in Figure 11 plots parallel to but slightly above the data for northern California. Given the overall steeper landscape in this part of the Oregon Coast Range one would expect the slightly higher values of watershed area for a given $\log(q/T)$.

There are two lines representing Coos Bay in **Figure 11**. The Coos Bay study site has been the subject of intensive field investigations for about 10 years (i.e. Montgomery et al., 1997, Andersen et al. 1997a, b). During this period, 35 landslides were mapped in a roughly 0.8 km² area (including those resulting from the November 1996 storms) (Montgomery et al., in prep.).

Two sources of topographic data were used. One was the digitized 7.5-minute USGS topographic map that was used to generate a digital elevation model with a 10-m grid, and the other was derived from airborne laser altimetry which was used to generate a digital elevation model with a 2-m grid. A shaded relief map derived from the laser altimetry is shown in **Figure 13**, and the mapped landslides are shown in **Figure 14**. A comparison of topographic maps for a portion of the study area is shown in **Figure 15**.

The difference in results between the two topographic data bases is substantial (**Figure 11**). Whereas the results using the 10-m resolution data fall close to the Elk Creek data, results for the 2-m resolution data plot very differently. In fact, using this latter data set, 94 percent of the landslides fell into the chronic instability category, which made up about 13 percent of the total watershed area. These results show that the model results strongly depend on the quality of the source of topographic data, and suggest that the amount of watershed area needed to account for a certain percentage of landslides should decrease significantly with increasing resolution of topographic data. A calculation using the Coos Bay site laser altimetry data and a form of SHALSTAB in which root strength is included (i.e., Dietrich et al. 1995) resulted in all of the landslides being accounted for within less than about 5 percent of the watershed area. Such a calculation is only practical when high resolution topographic data are available.

Our validation study fulfilled two purposes. First, the study was designed to evaluate whether SHALSTAB correctly identifies areas of a watershed that are more prone to shallow landsliding. The results presented strongly support the usefulness of the model for this purpose. In all cases, landslide density was much greater in the most unstable categories than in the more stable ones, and much greater than that which was obtained with the random placement model. Overall, this validation test was a stringent one. Any operational bias was avoided because each phase of the analysis was done by a different individual, i.e., the aerial photographic interpretation, SHALSTAB modeling, and comparison of the two data sets were each done by different people. No effort was made to make the model fit the data.

The comparison with the random model is particularly important. Although for most cases the observed landslide density is no better than the random model for $\log(q/T)$ of -3.1 to -2.8, this does not mean that areas characterized with this instability category are not highly unstable. It just means that we could not distinguish the frequency of landslides which fell in this category from random. Recall, however, that the random data also have the bias of selecting the lowest q/T value to represent the instability. This was necessary to match the operational procedure for mapping the observed landslides. No such bias, however, occurs randomly in nature, instead steeper slopes are more unstable because it takes less water to destabilize them. Hence, our random model procedure tends to produce results which are biased towards naturally less stable slopes. When the slides are associated only with one cell, this bias would be eliminated (as shown in Figure 12 for the Elk Creek data of Oregon), and model differences from random may more commonly extend to the $\log(q/T)$ value of -2.5.

The results show that the performance of SHALSTAB depended strongly on the quality of the topographic data (as illustrated above with the Coos Bay data). Although we used the best available topographic data (data digitized from USGS 7.5-minute maps), these maps systematically miss the finer scale topographic features that dictate where shallow landslides occur. This results in a landscape that is smoother, meaning that there are fewer areas of high convergence (i.e., smaller a/b) because the finer scale valleys are missed. The landscape also appears less steep on these maps. Both of these deficiencies strongly affect the accuracy of the SHALSTAB predictions. They also make mapping of observed landslides (either from aerial photographs or in the field) less accurate. Despite these drawbacks, SHALSTAB successfully delineated areas where shallow landslides most commonly occurred.

The second aspect of the validation study is the assignment of landslide hazard or "risk" to each instability category. Without the benefit of a validation study, we treated the categories of chronic and $\log(q/T) < -3.1$ as high hazard areas for the purposes of restricting forest management activities. The data presented here clearly support the use of these two categories to delineate the highest risk areas. Furthermore, L-P treats the inner gorge area as high hazard, and, as shown in **Table 5a**, including the inner gorge area substantially increased the percentage

of the mapped landslides that fell into the high hazard category. The percentage of the total area rated as high hazard also increased up to 22 percent. Inspection of Tables 5a and 5b suggests that if a target number of landslides or volume of landslides was set, the threshold $\log(q/T)$ for high hazard could vary among the watersheds. In general, however, such data for individual watersheds are not available, hence a single threshold value for most lands will be used. If the threshold were increased for all watersheds to -2.8, there would be a significant increase in the percent of landslides (by number or volume) included in the high hazard area. If the inner gorge areas are not included, then on average the increase from -3.1 to -2.8 as a threshold increases the area mapped as high hazard by a factor of 1.6.

This study was designed to test the basic validity of the model and to explore the effects of using different $\log(q/T)$ thresholds to define high hazard areas. It was not designed, however, to determine the most appropriate threshold to use in defining high hazard areas. We recommend that the $\log(q/T) = -3.1$ (plus inner gorge) be accepted as the high hazard area, but that during field trials by geotechnical specialists in Timber Harvesting Plan (THP) preparation, that the map area for review include the sites with $\log(q/T) \wedge -2.8$. After several plans are prepared it should become apparent to the specialist whether the extra work needed to inspect sites with $\log(q/T)$ values between -3.1 and -2.8 is unnecessarily burdensome or in fact reveals sites that should be treated as high landslide potential.

A few comments about use of the hazard maps should be made. The maps are created to provide an overview of potential landslide hazards so that operational constraints imposed by the risk of landsliding can be incorporated into watershed and regional land management decisions. The maps do not replace field work. Instead, the maps should be viewed as hypotheses to direct field inspections by specialists. Such field inspections should not be restricted, however, to just determining whether areas delimited by the model as high hazard appear to be so on the ground. Errors of exclusion also occur (i.e. unstable areas exist which are missed by the model). Hence, during field inspection the specialist should also note areas that should be mapped as high hazard but are not identified by the model. In essence, then, the model results serve the function in the field of directing the specialist's observations and challenging the specialist to create a defensible alternative analysis. Besides the obvious limitations imposed by inferior topographic data, SHALSTAB also does not account for many things we know can matter to slope instability such as mechanically weak rocks, springs, locally high or low root strength and soil thickness, to name a few. The underlying hypothesis in using SHALSTAB (now supported with this validation study) is that the model predictions can account for the majority of shallow landslides found across the landscape. We strongly recommend a systematic effort to record THP reviews by specialists to document how well the field inspections support the use of SHALSTAB digital terrain predictions.

Defining thresholds to use in management decisions is not a purely scientific process. Resource managers must treat this as an exercise in risk management. L-P currently plans to collect more information about shallow landslides, sediment budgets, and tolerances of aquatic habitats to sediment loading through the use of intensive watershed analysis in selected watersheds. These studies, combined with the current validation study should provide foresters and land managers with better information on which to base risk management decisions regarding shallow landslide hazards. Future decisions should also consider the utility of using higher resolution topographic data generated by laser altimetry surveys to improve the accuracy of SHALSTAB.

Acknowledgments

This study was funded by Louisiana-Pacific (L-P) and Stillwater Sciences. We would like to thank the following L-P staff for their support during this project: Jim Lemieux and Malcom Pious for helping secure the initial funding and for their encouragement throughout the study, and Chris Surfleet for assisting in the field surveys and for reviewing an earlier draft of this report.

References Cited

- Dietrich, W.E., C.J. Wilson, D.R. Montgomery, J. McKean, and R. Bauer. 1992, Erosion thresholds and land surface morphology, *Geology*, v. 20. p. 675-679.
- Dietrich, W.E., C.J. Wilson, D.R. Montgomery, and J. McKean, 1993, Analysis of erosion thresholds, channel networks and landscape morphology using a digital terrain model, *J. Geology*, Vol. 101, No.2, p.161-180.
- Dietrich, W.E., Reiss, R., Hsu, M., and Montgomery, D.R., 1995. A process-based model for colluvial soil depth and shallow landsliding using digital elevation data, *Hydrological Processes*, Vol. 9, 383-400.
- Dietrich, W. E., and D. R. Montgomery, 1998, Hillslopes. channels and landscape scale. G. Sposito, editor, *Scale dependence and scale invariance in hydrology*, Cambridge University Press, Cambridge, England.
- Montgomery, D. R. and W.E. Dietrich, 1994, A physically-based model for topographic control on shallow landsliding. *Water Resources Research*, vol.30, no.4, p.1153-1171..
- Montgomery, D.R., W. E. Dietrich, R. Torres, S. P. Anderson and J. T. Heffner, 1997. Hydrologic response of a steep unchanneled valley to natural and applied rainfall, *Water Resources Research*, vol. 33, no.1, p. 91-109.
- Montgomery, D.'R., W. E. Dietrich, and K. Sullivan, 1998, The role of GIS in watershed analysis. *in* S. N. Lane, K. S. Richards and J. H. Chandler, editor, *Landform monitoring, modeling and analysis*, John Wiley & Sons Ltd. P.241-261.
- Spittler, T. E., 1995, Pilot monitoring program—geologic input for the hillslope component, California Department of Conservation, Division of Mines and Geology.
- WFPB (Washington Forest Practice Board), 1993, Standard methodology for conducting watershed analysis. Version 2.0, 85pp.
- Wilson, C.J. and W.E. Dietrich, 1987, The contribution of bedrock groundwater flow to storm runoff and high pore pressure development in hollows. *Proc. Int. Symp. on Erosion and Sedimentation in the Pacific Rim. 3-7 August 1987, Corvallis. Ore., Int. Assoc. Hydrological Sciences Bull., Pub. no. 165, p. 49-59.*

Figure 2a

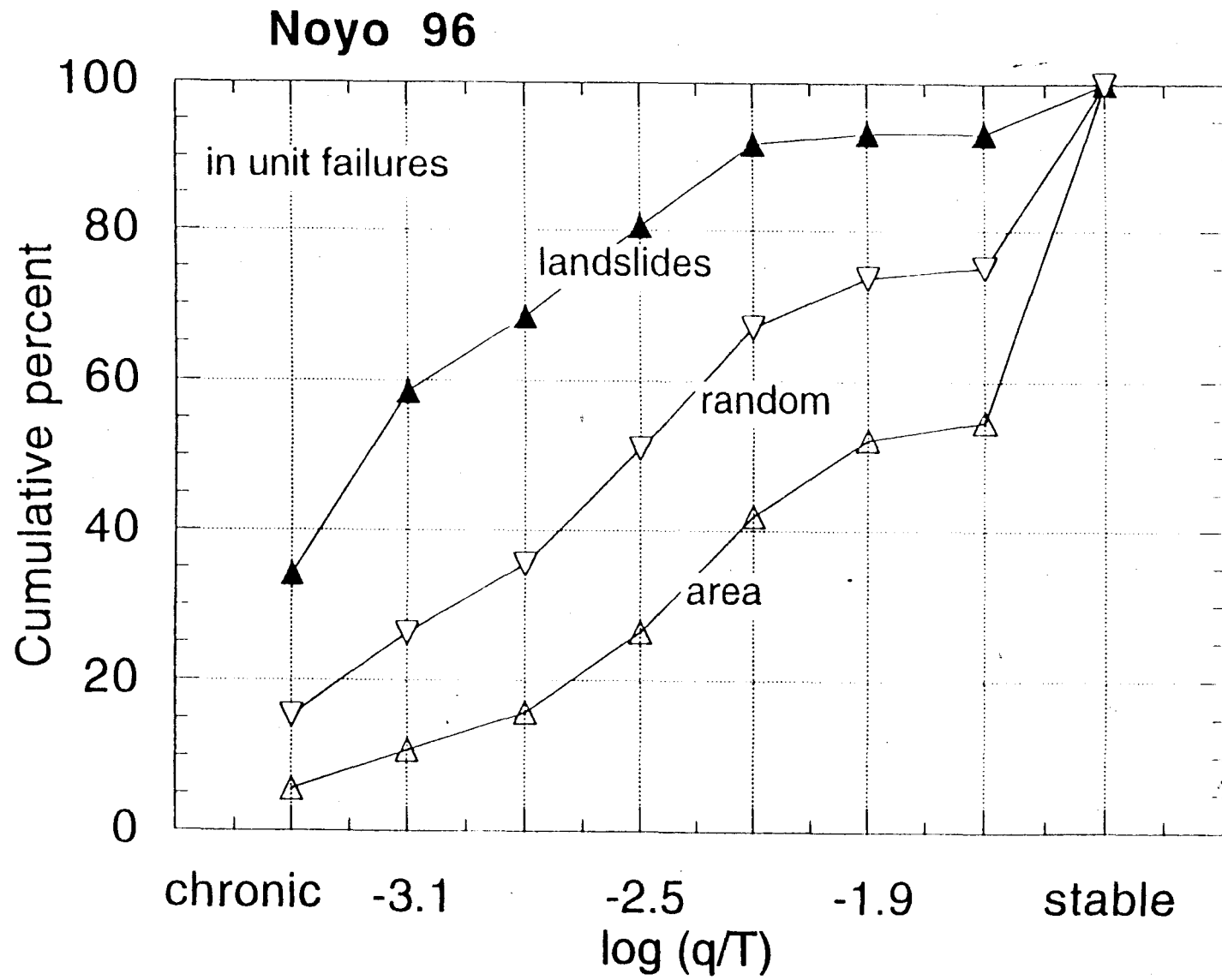


Figure 2b

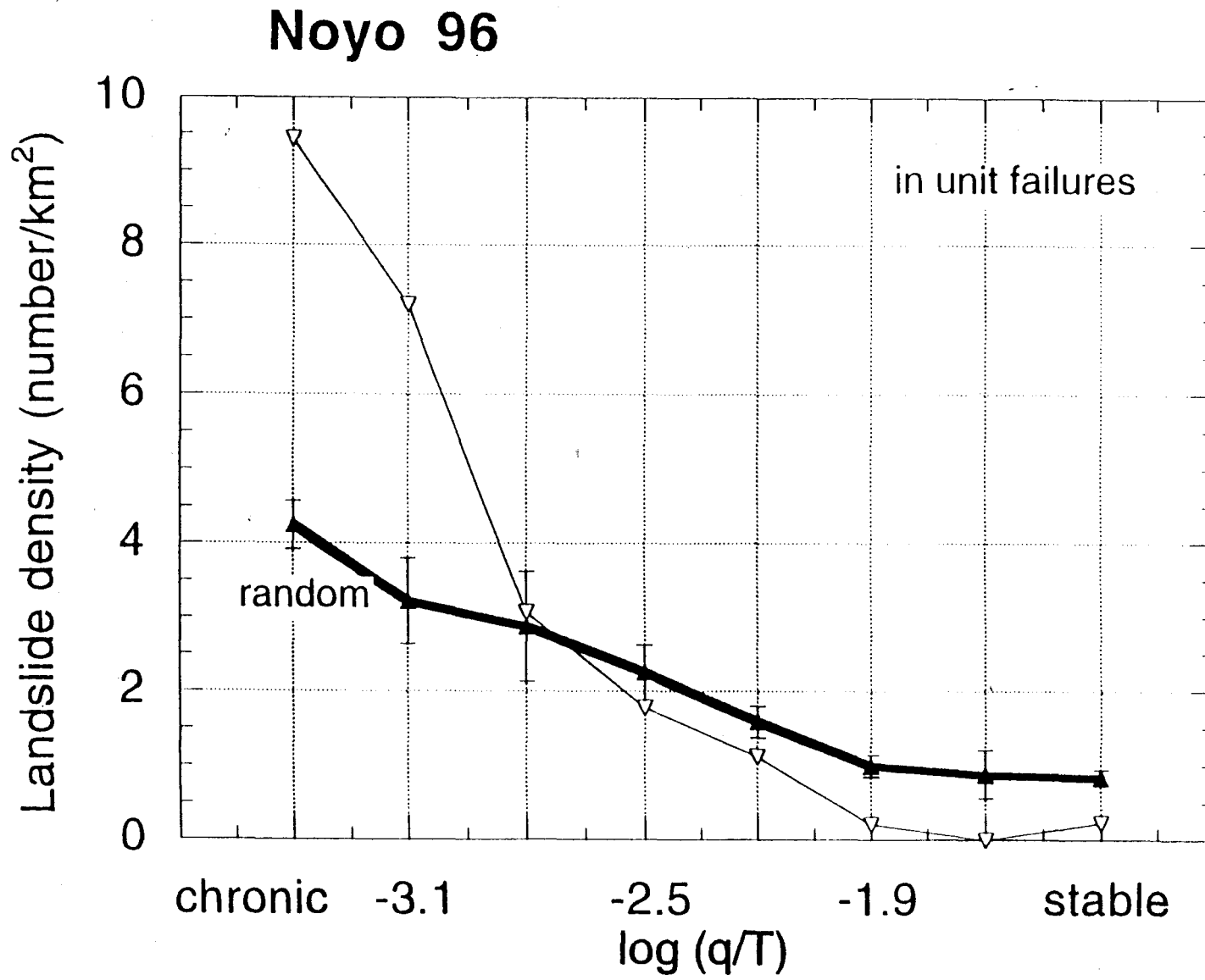


Figure 2c

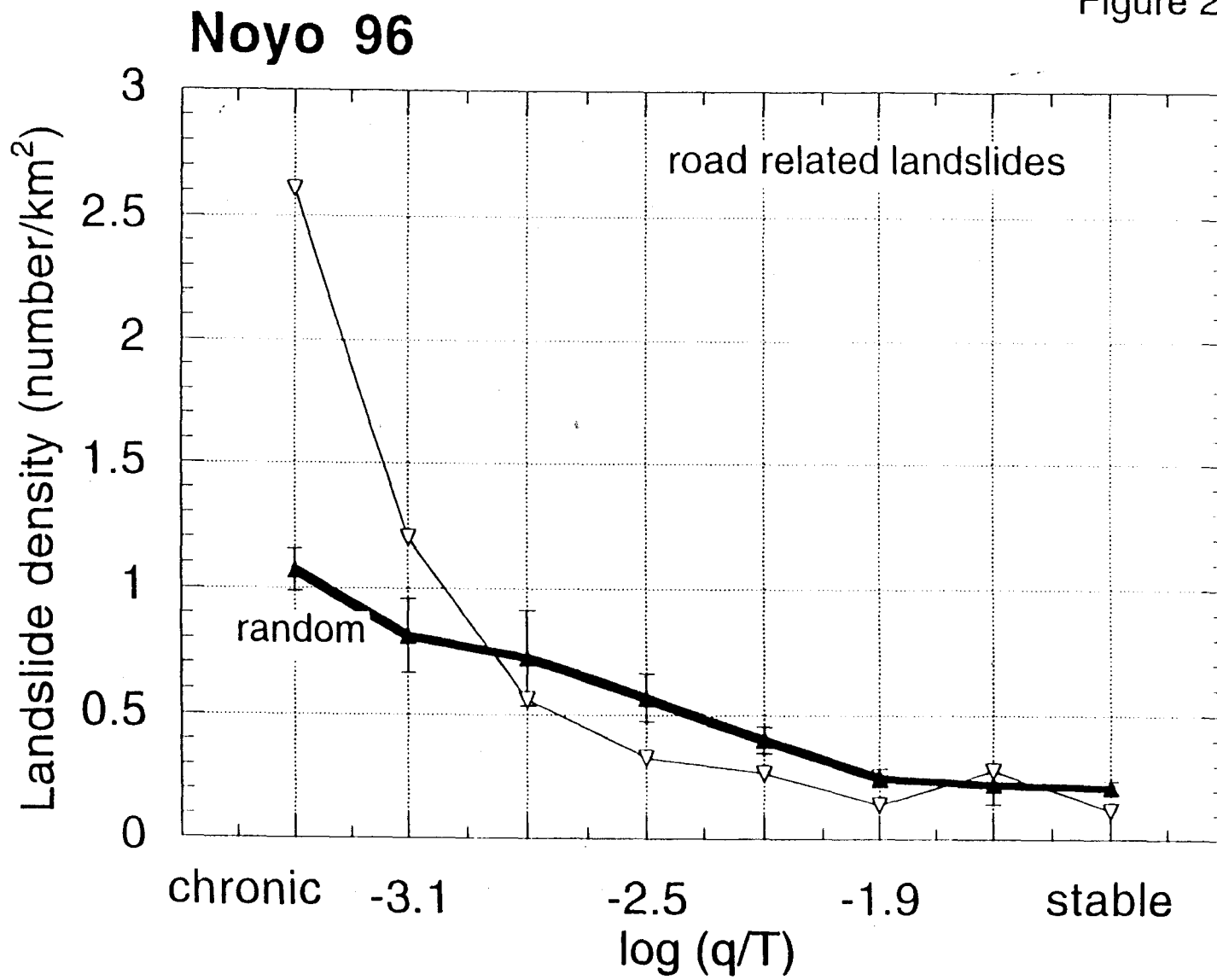


Figure 8

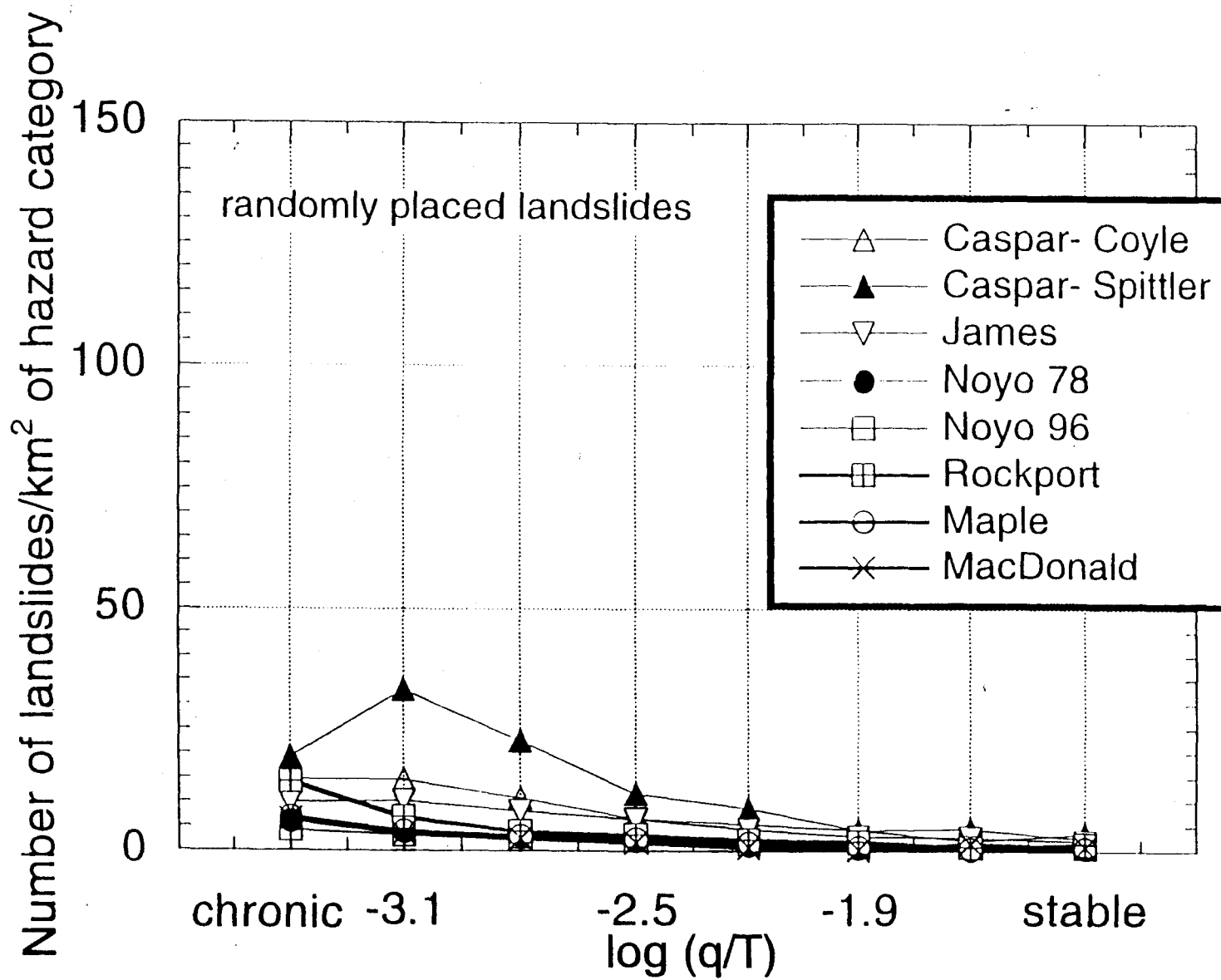


Figure 5

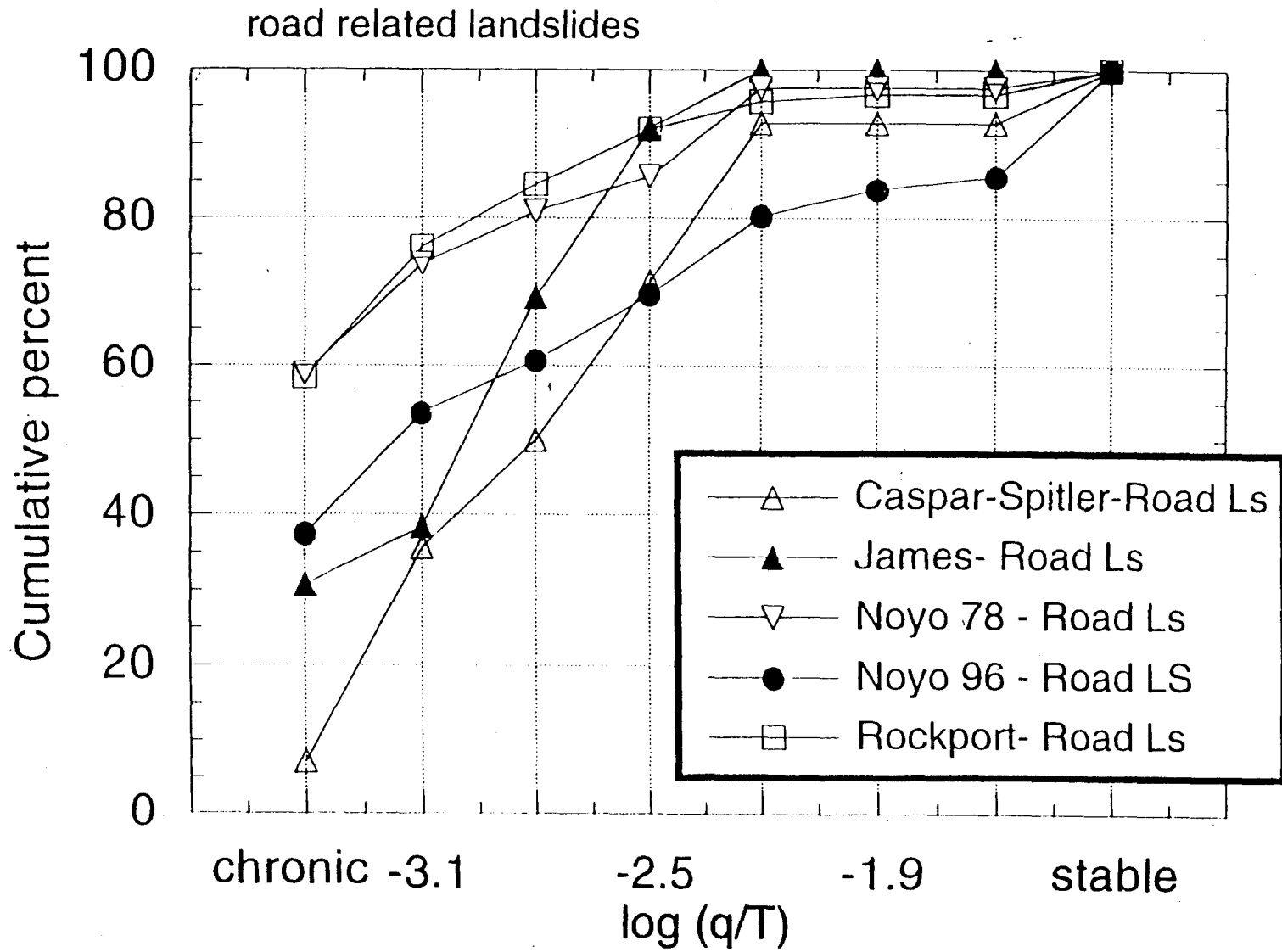


Figure 6a

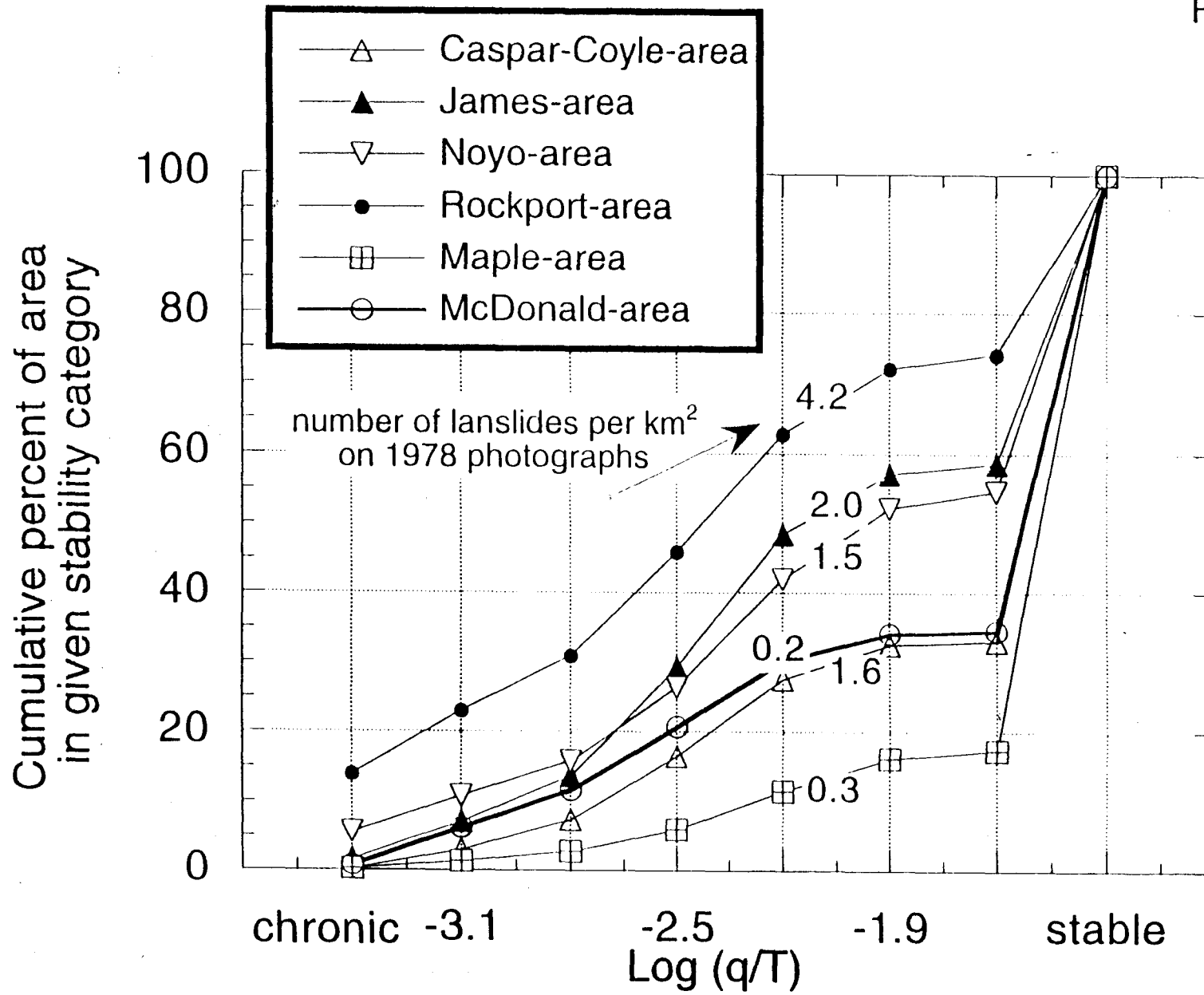


Figure 6b

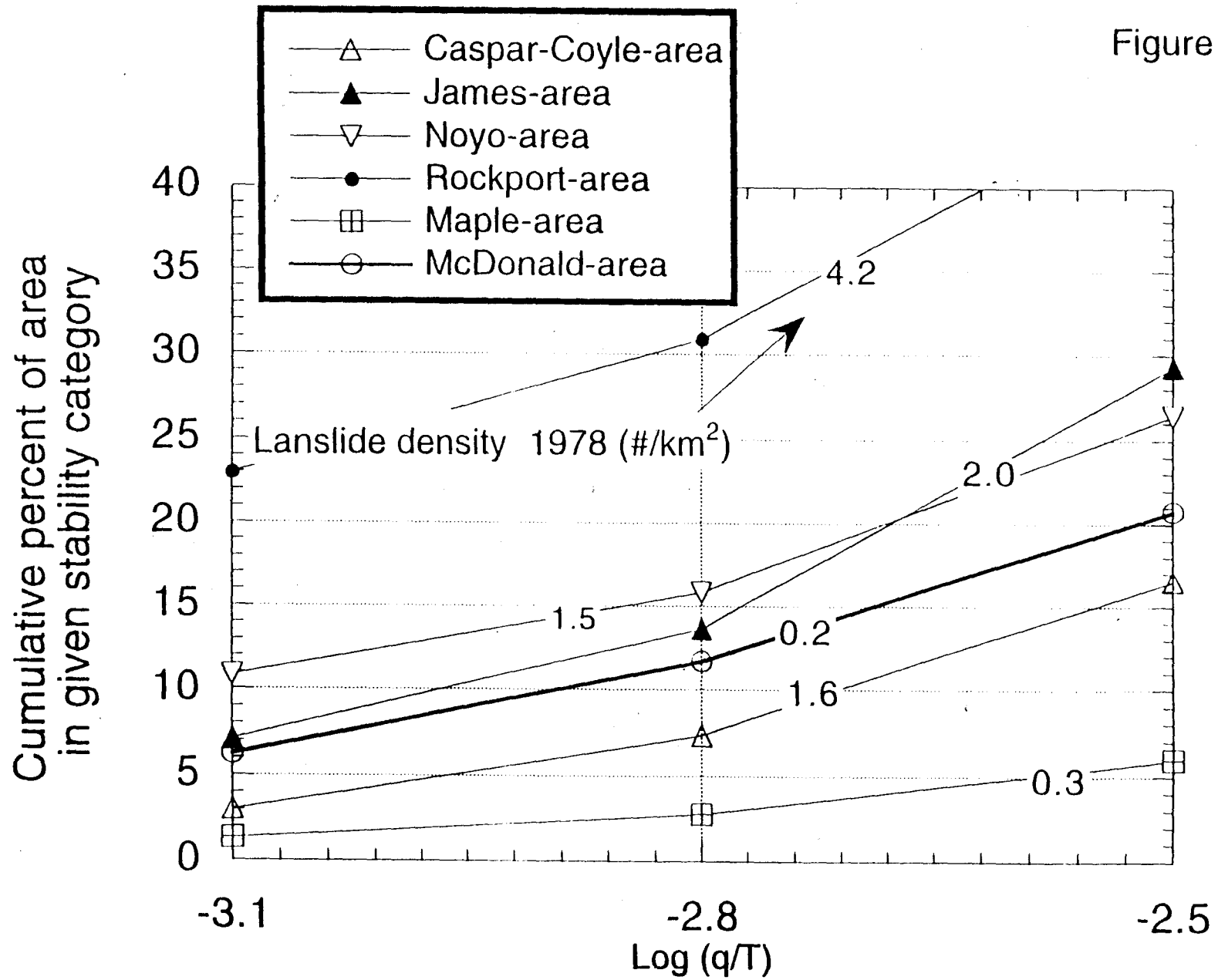


Figure 7

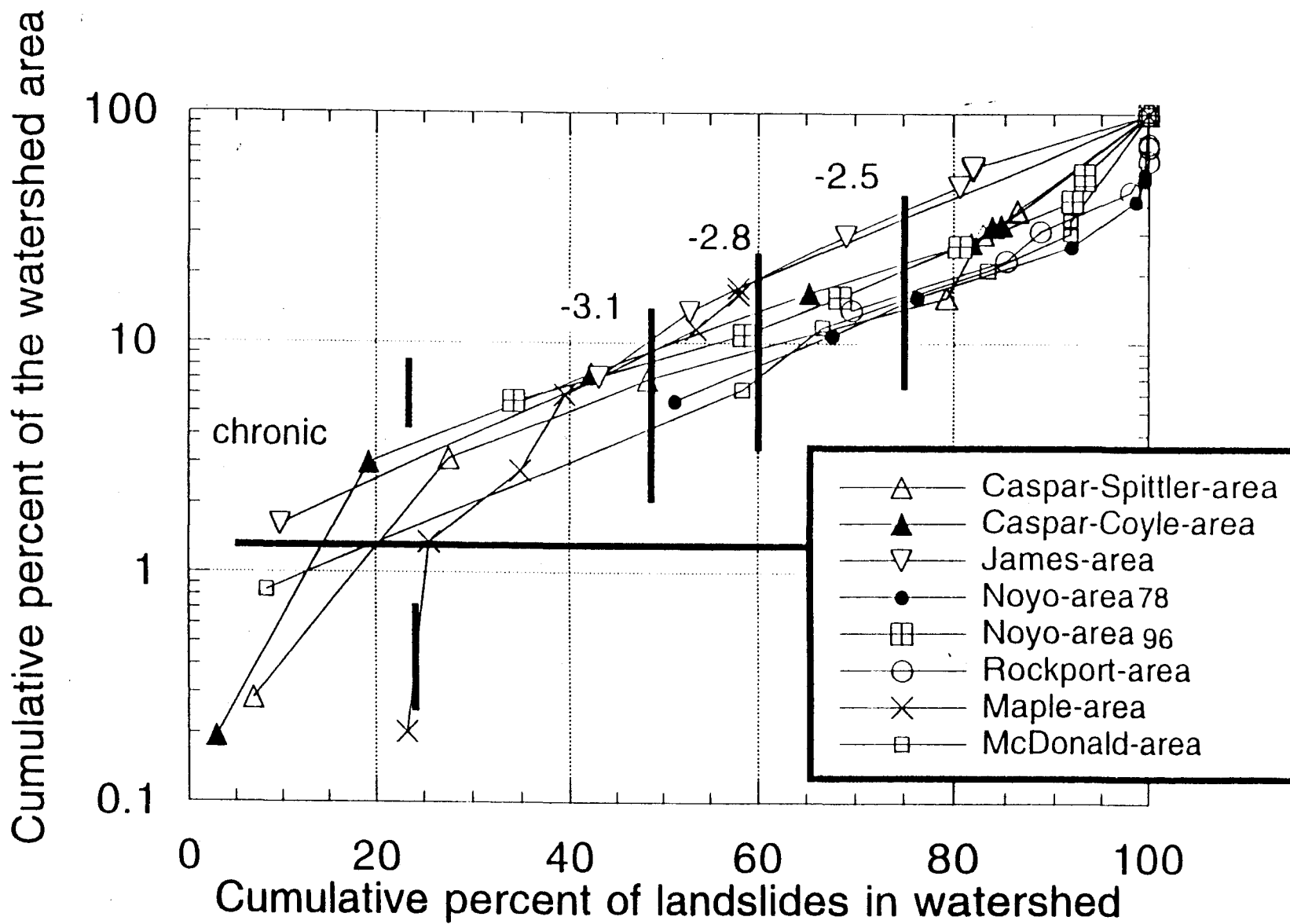


Figure 8

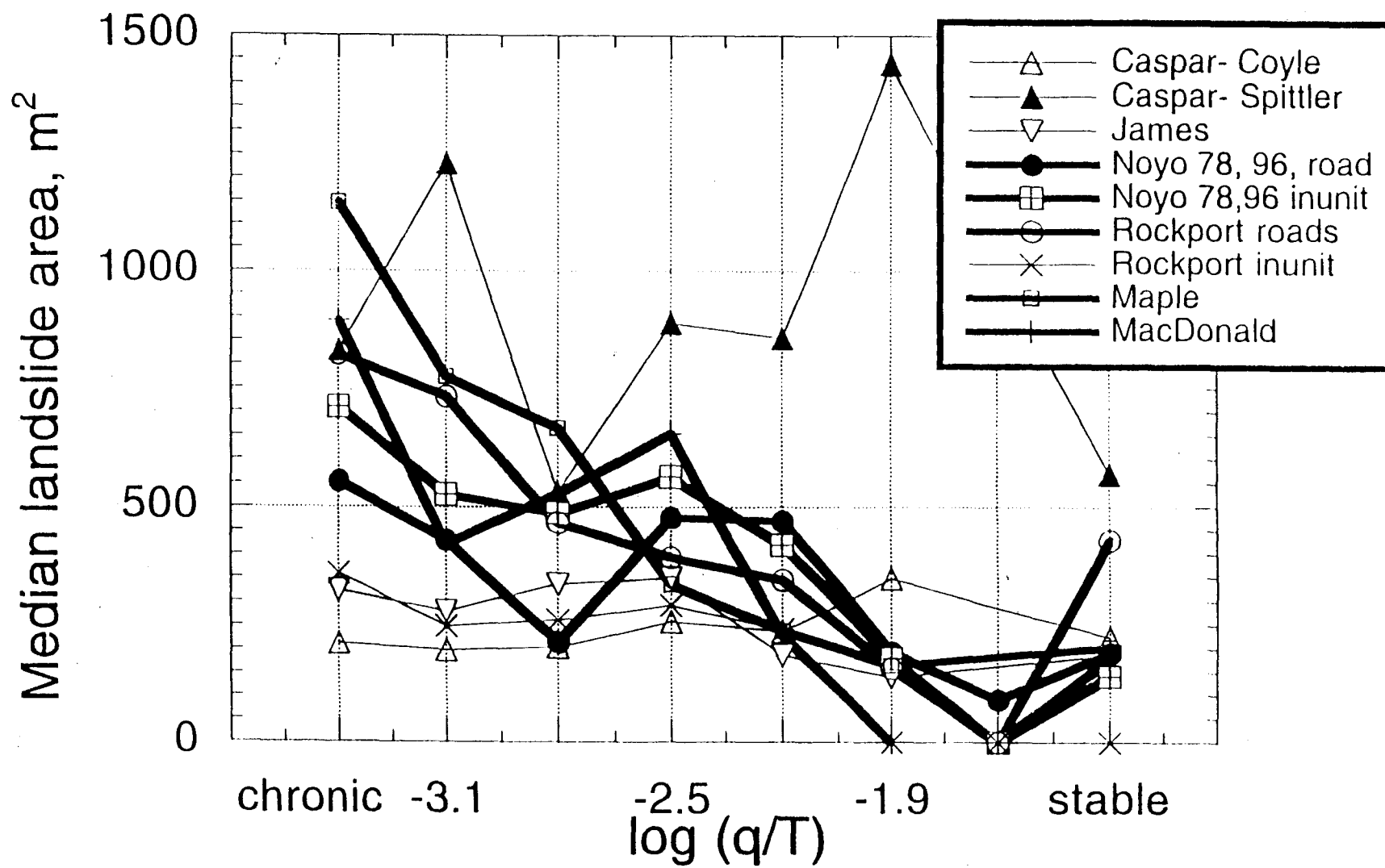


Figure 9a

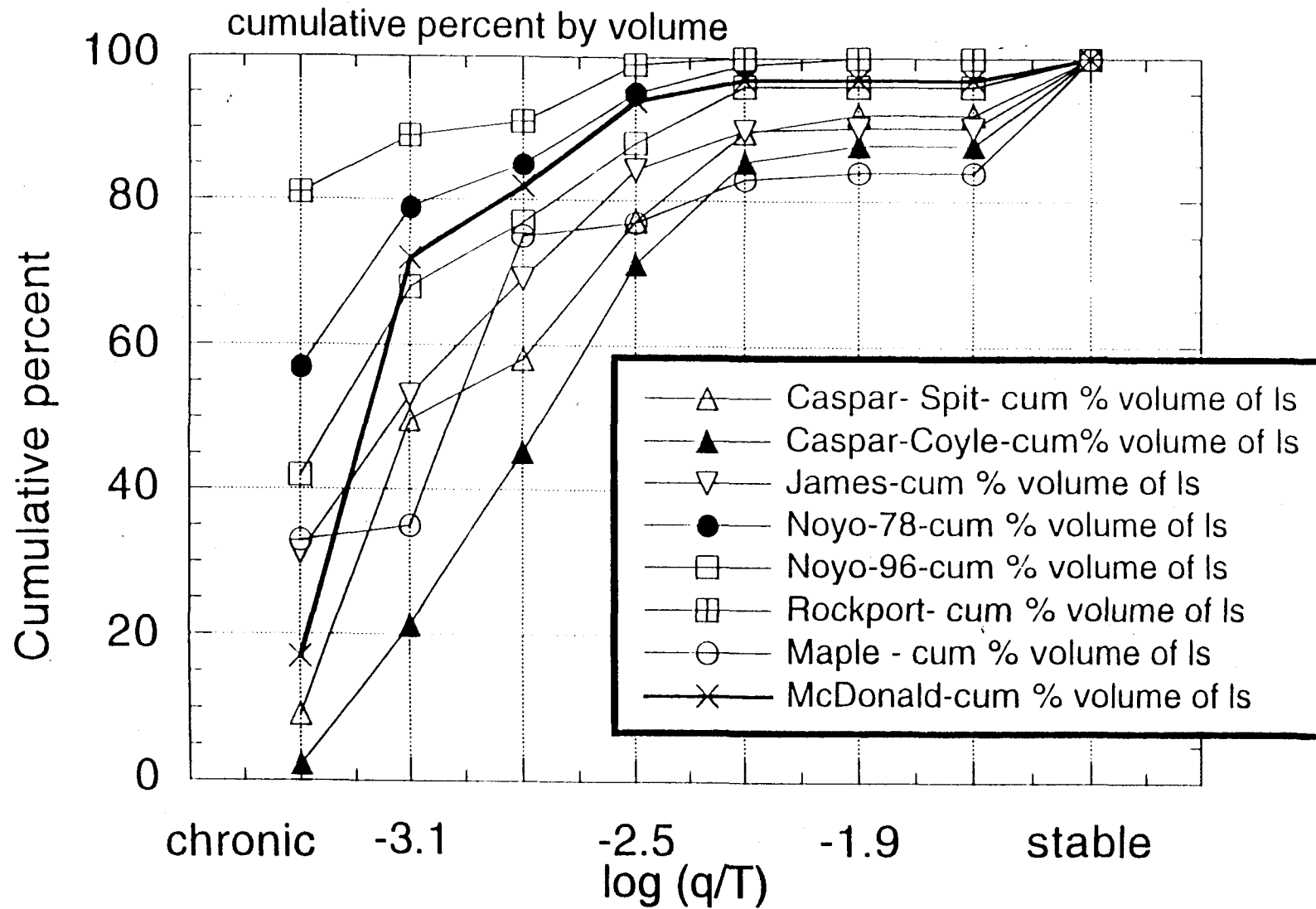


Figure 9b

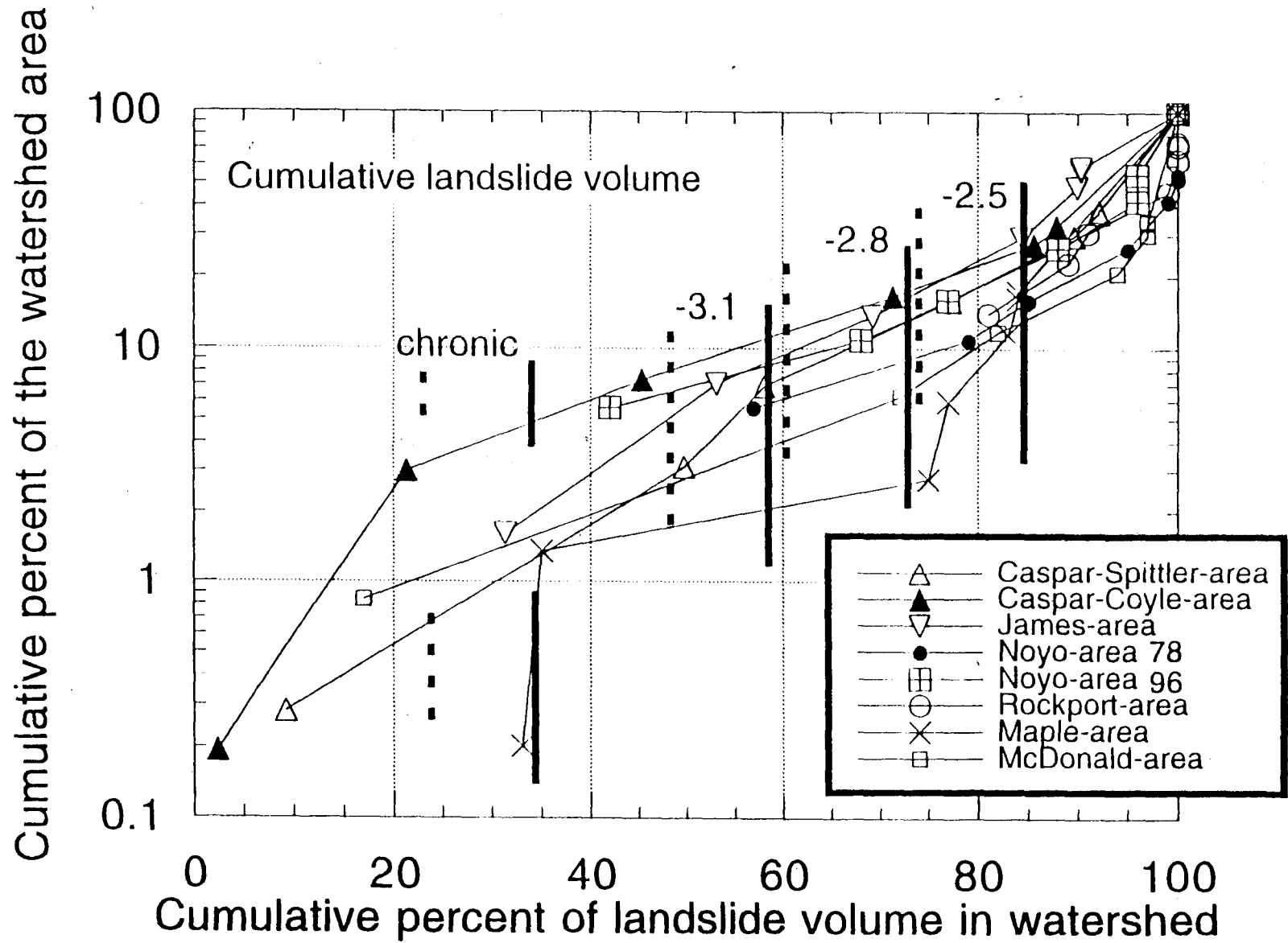


Figure 10

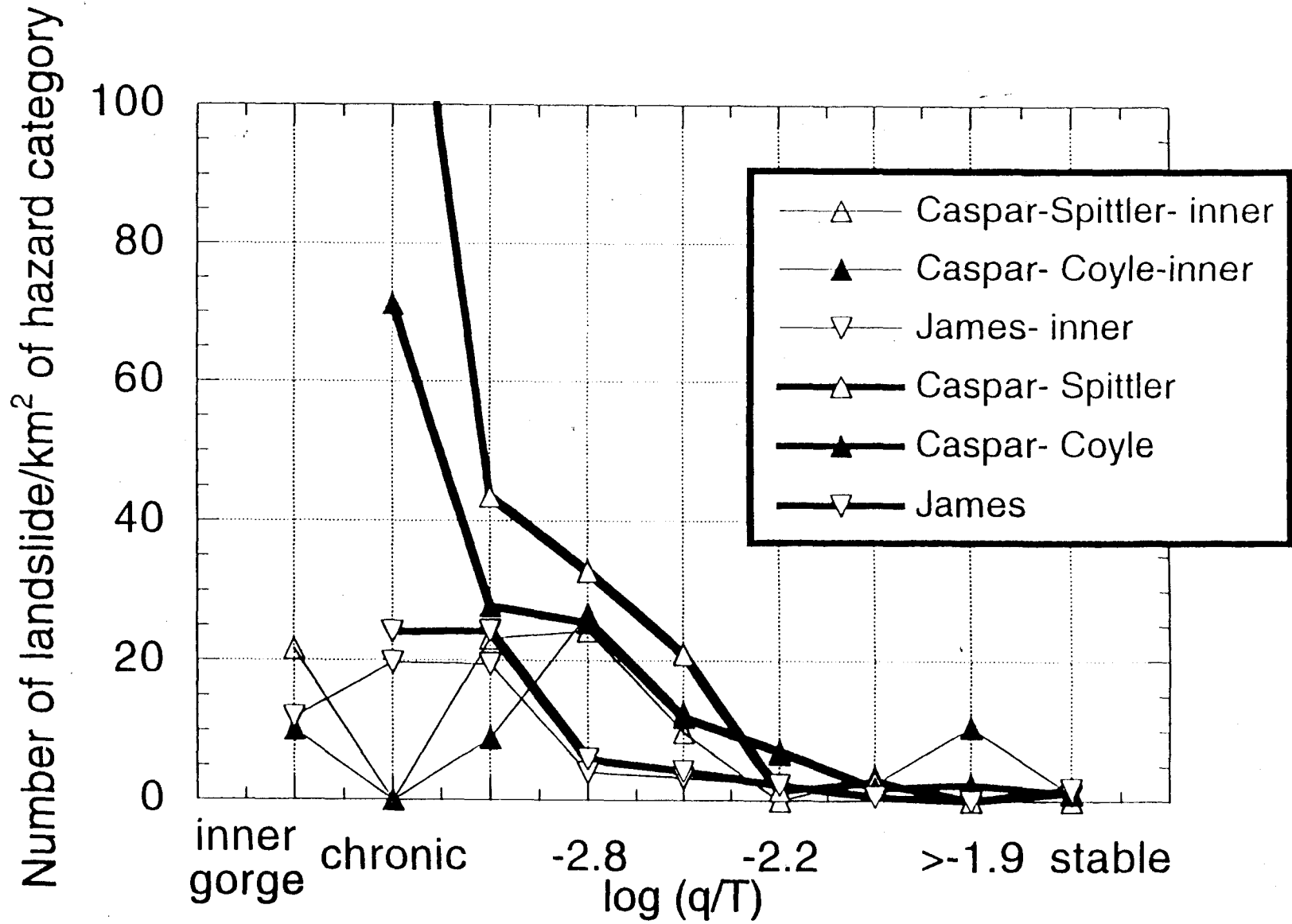


Figure 11

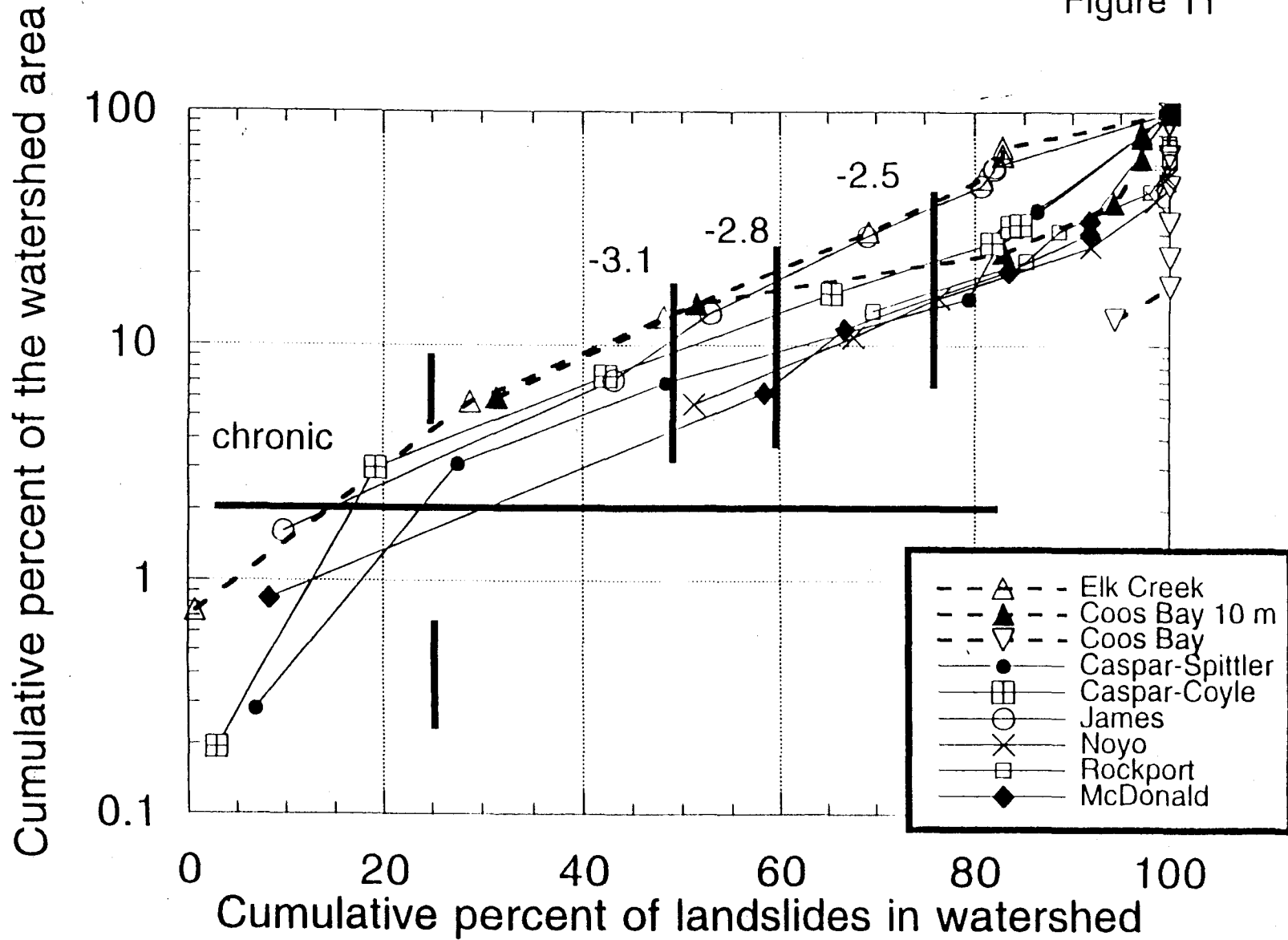
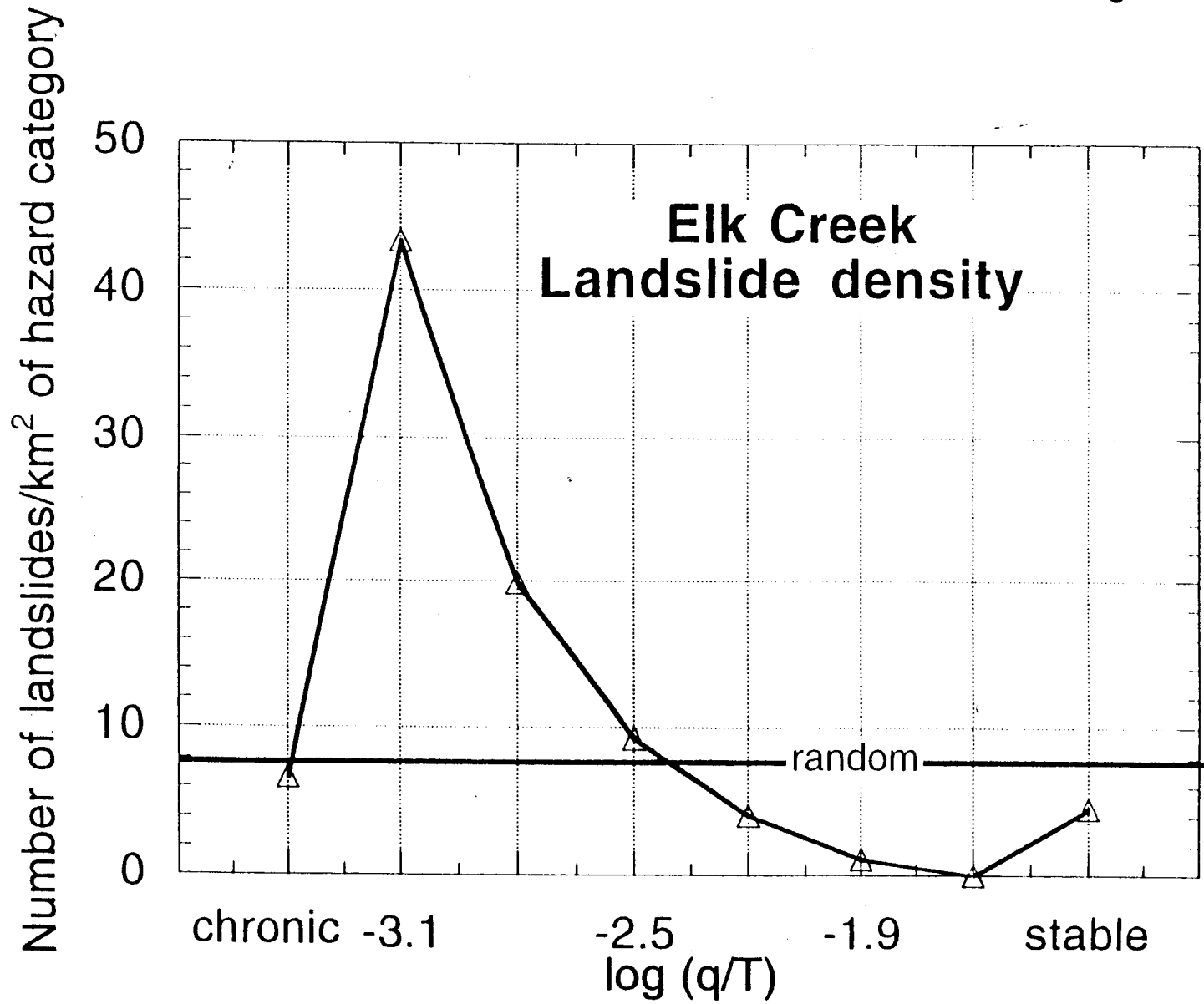


Figure 12



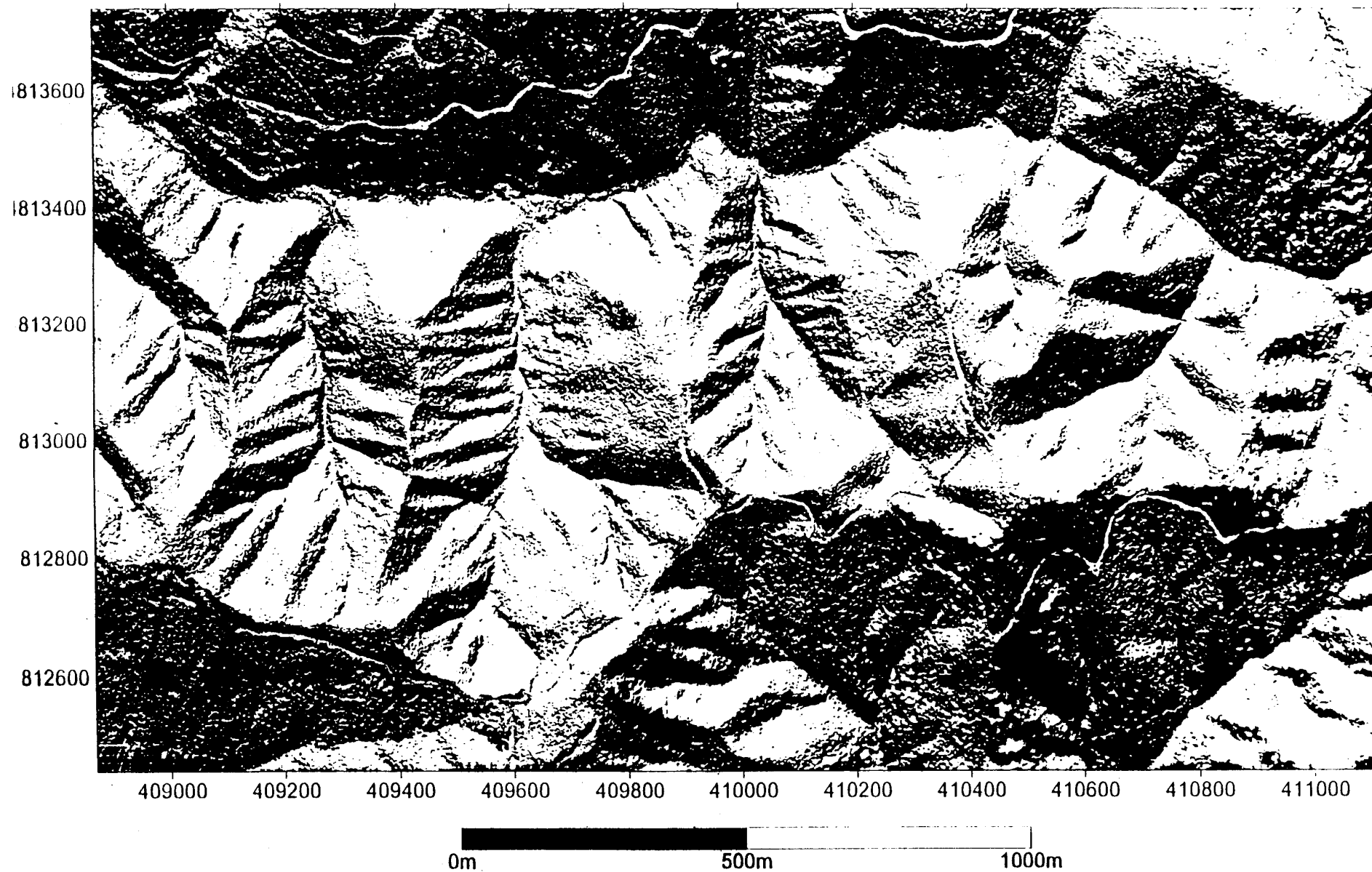
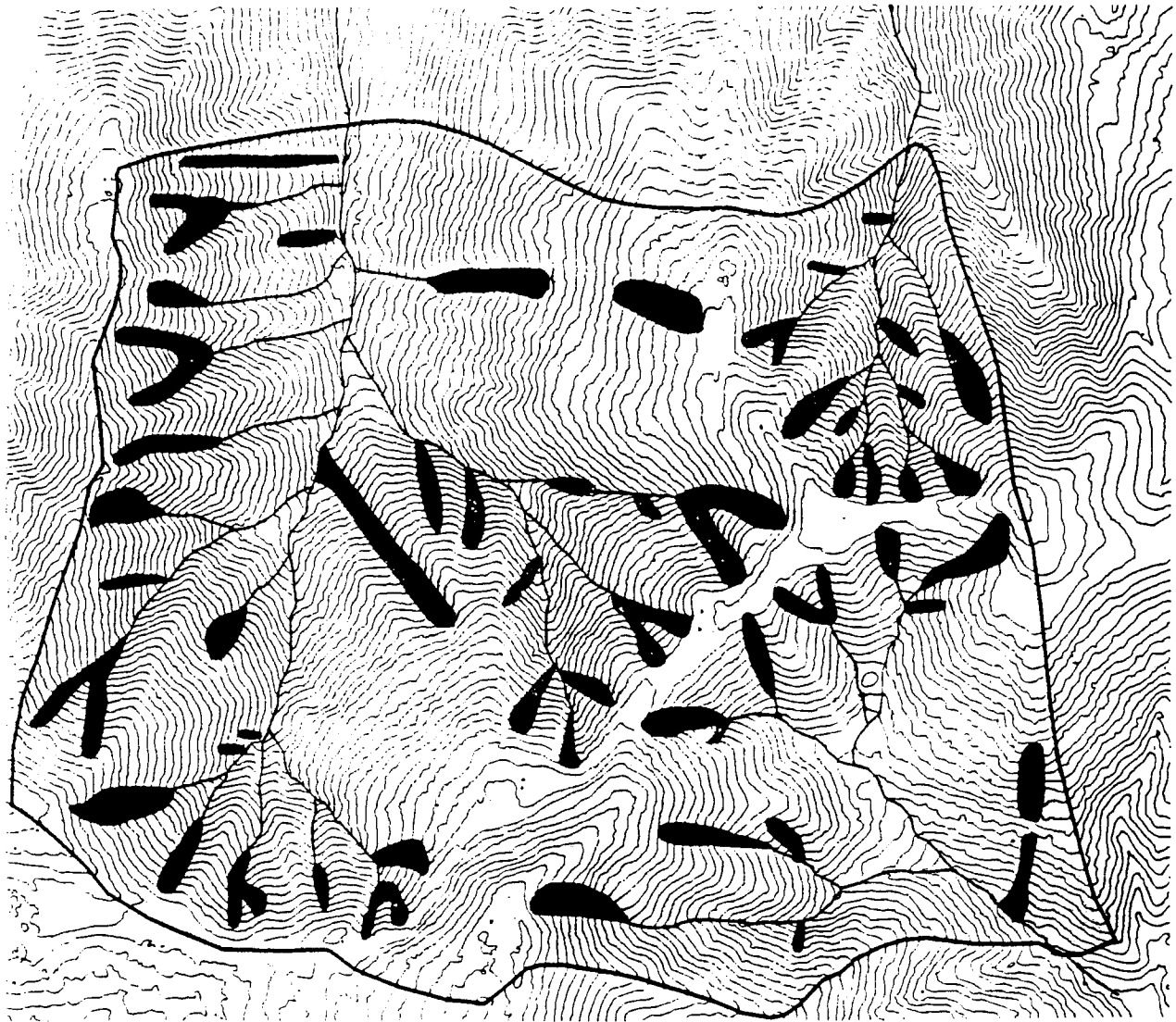


FIGURE 13



0 800 m

Contours: 5m, Grid: 2m

- Landslide Scars
- Thick Colluvium in Hollow
- Mapped Area
- Channels
- Boundary of Mapped Area

FIGURE 14

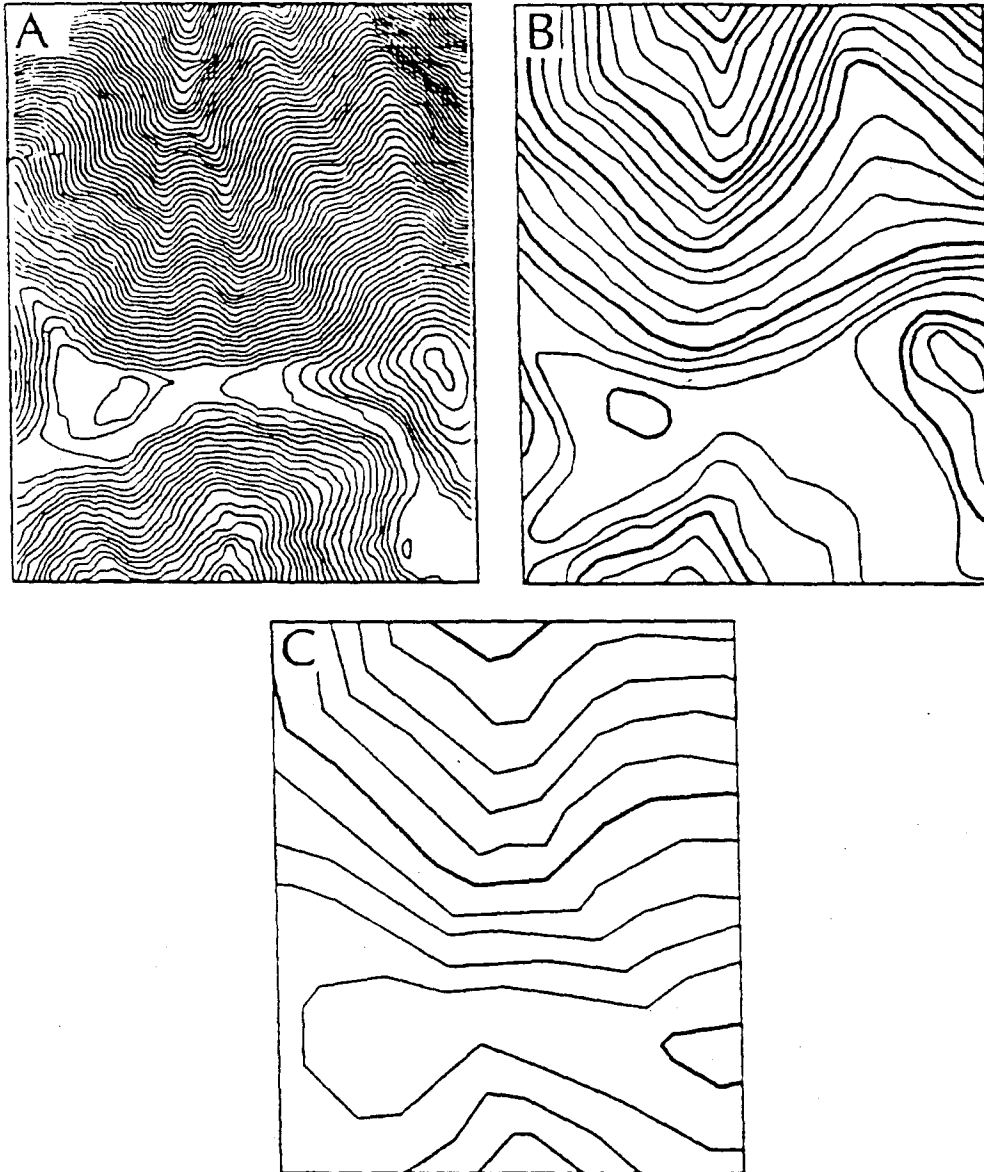


Figure 15. Topographic contours for a small valley along Mettman Ridge, near Coos Bay, Oregon, from maps of different scales that illustrate the effect of topographic resolution on the portrayal of hillslope length, and thus drainage density. For each map, north is toward the top of the figure, and the width of the panel is 200m. (A) Map created from laser altimetry data obtained from a low flying plane (individual survey points were, on average, 2.6 meters apart); contour interval, 20 ft (6.1 m). (B) Map derived from aerial photographs and originally plotted at 1 : 4,800 scale by Weyerhaeuser Company; contour interval 20 ft (6.1 m). (C) Map derived from aerial photographs and originally plotted at 1 : 24,000 as part of the USGS 7.5' Allegheny quadrangle; contour interval 40 ft (12.1 m). Note that the five fine-scale valleys apparent on the field-survey map are reduced to one or two distinct valleys on the coarser-scale maps and that the apparent zone of hillslope convexity increases with map scale.

(from Dietrich and Montgomery, 1998)

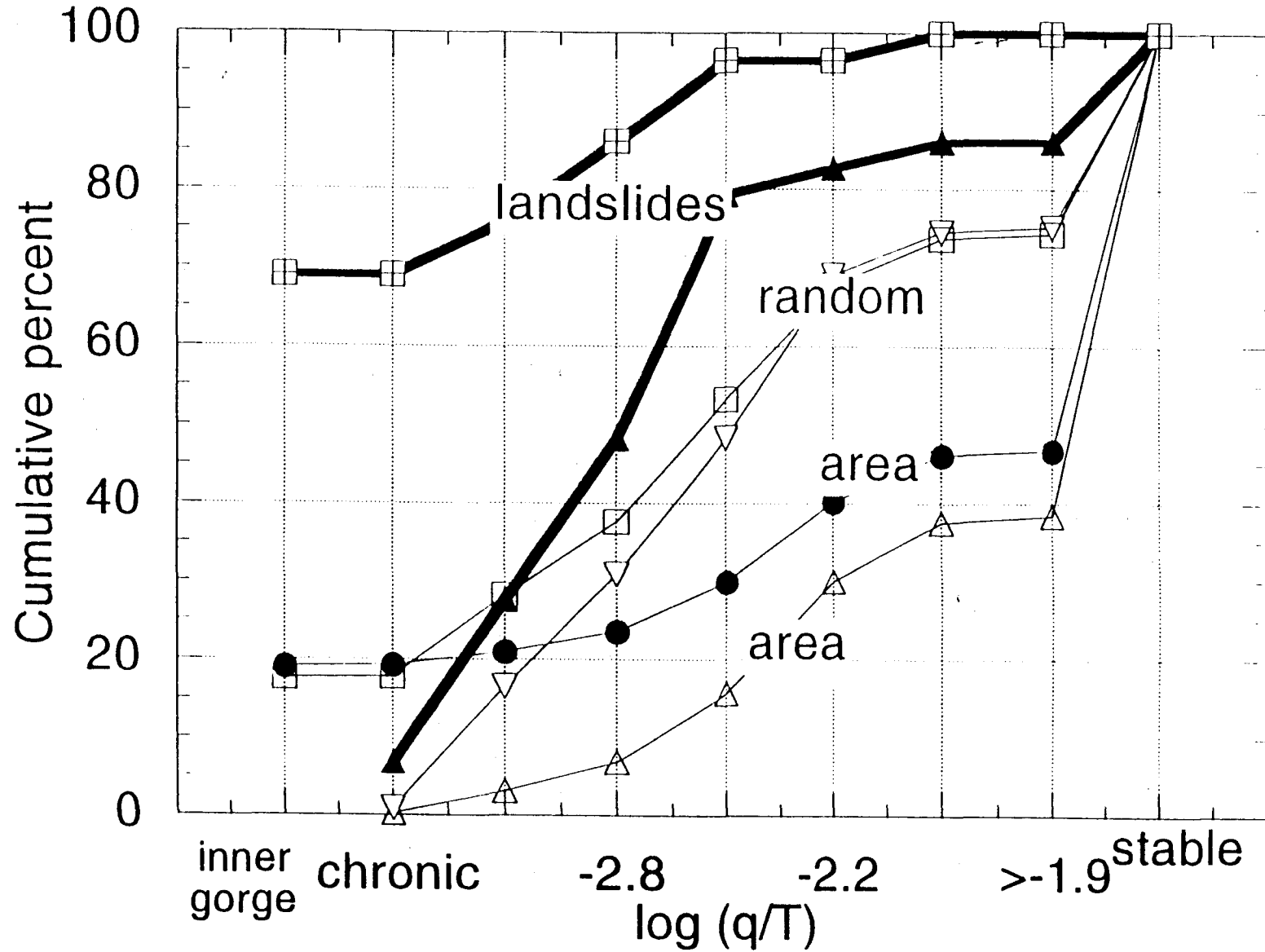
Appendix

Individual plots for each watershed of: 1) cumulative percent area, landslide number and random number and 2) landslide density.

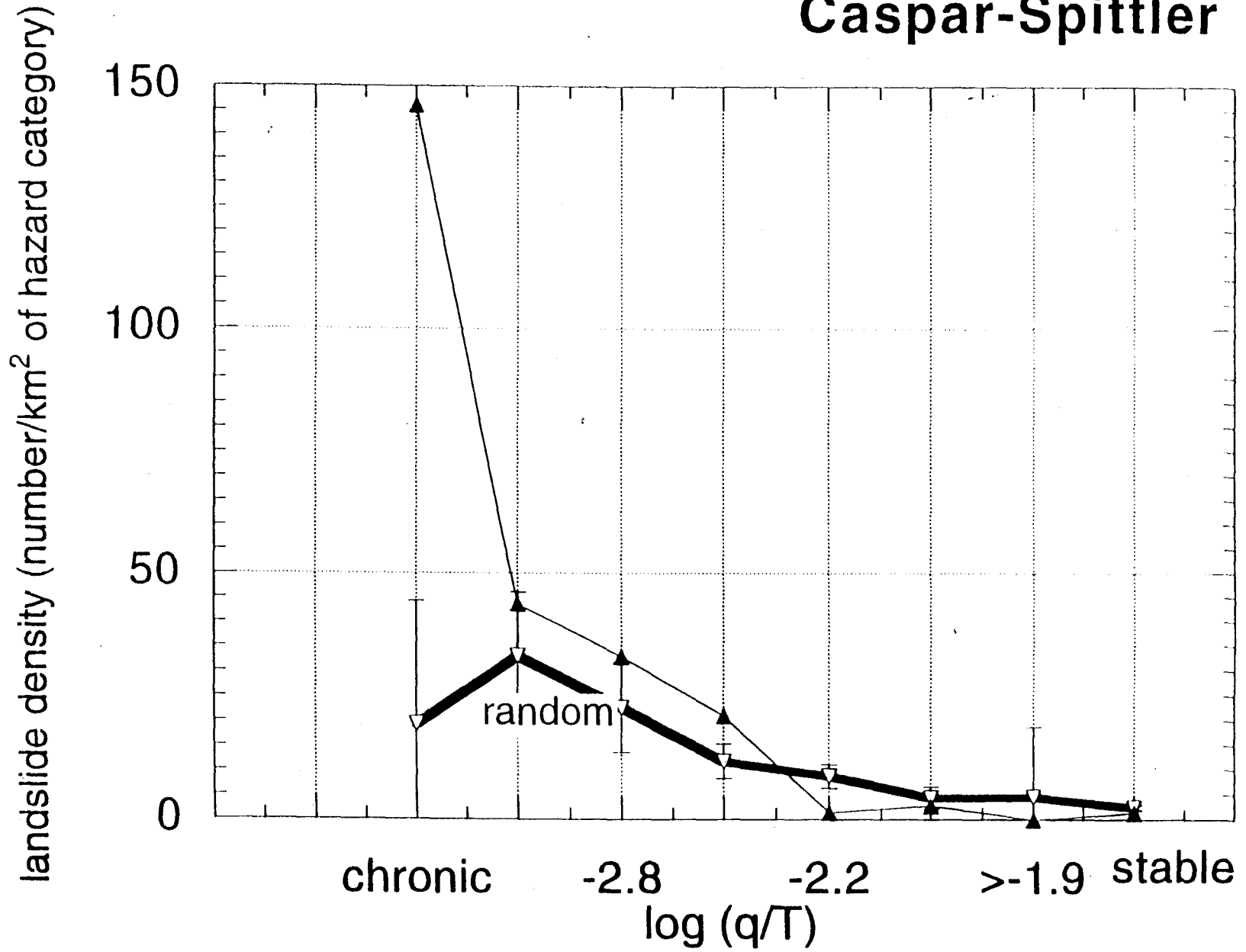
Plots of results of study sites in Oregon

Maps of the pattern of $\log(q/T)$ and landslide location for each watershed

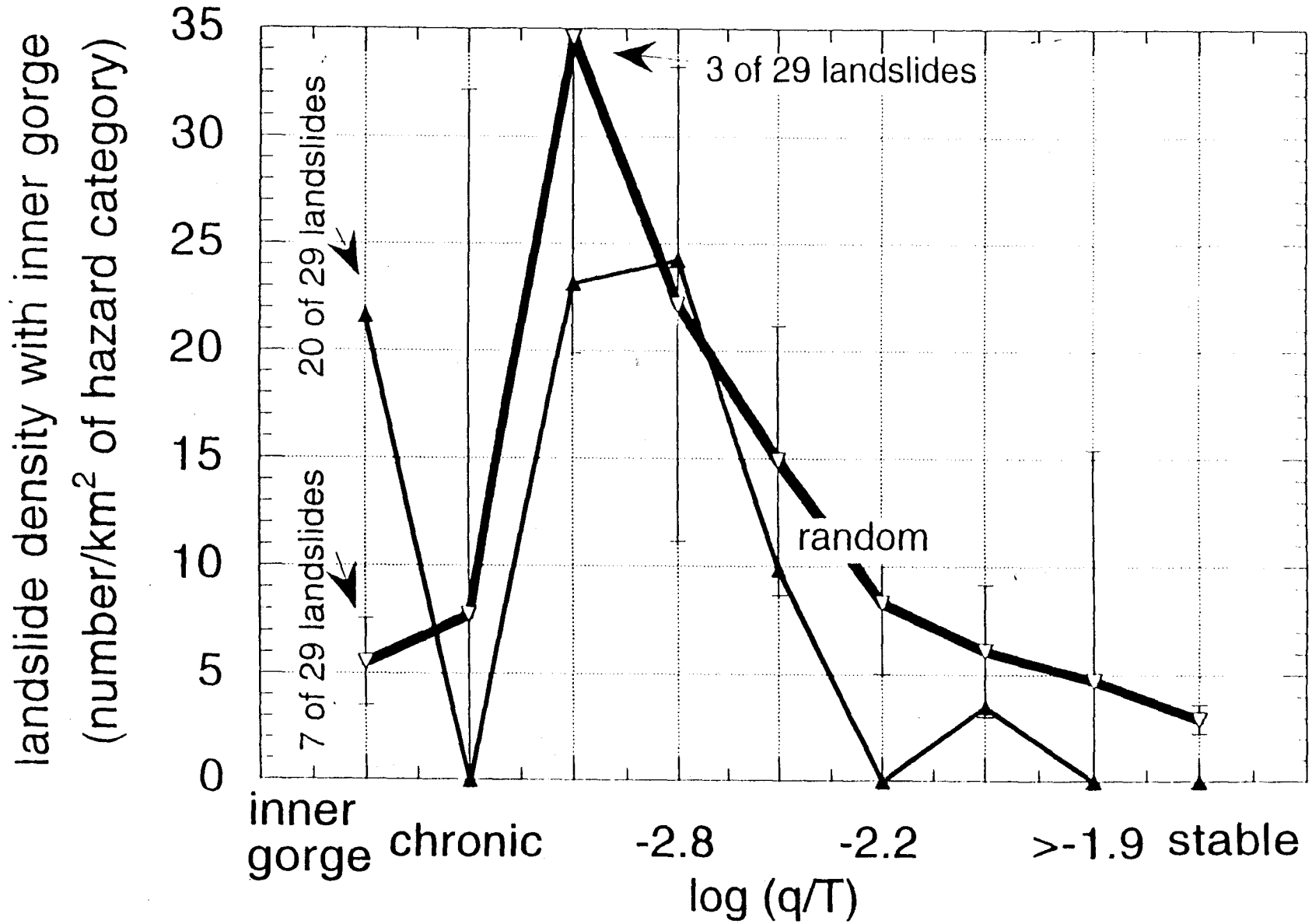
Caspar-Spittler



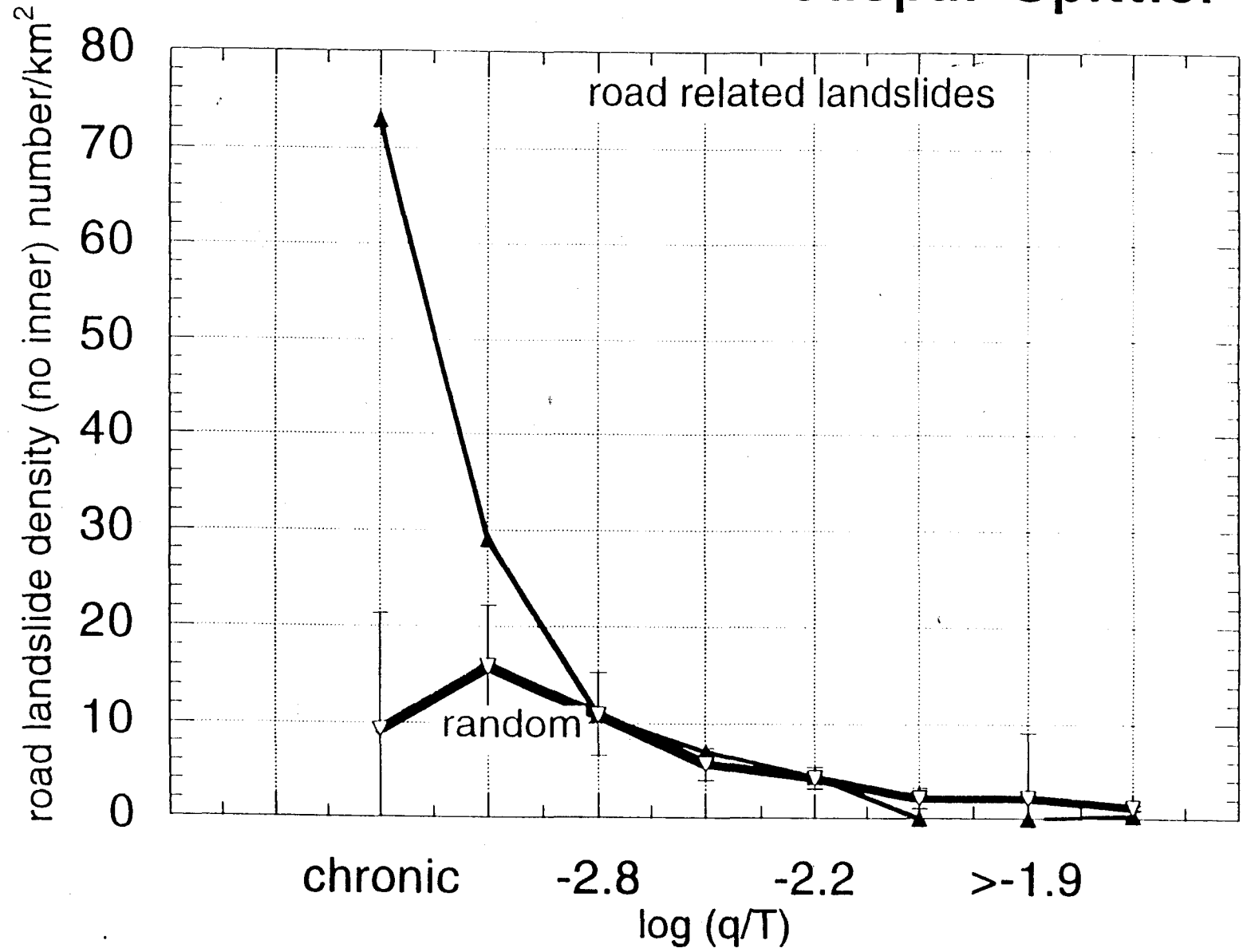
Caspar-Spittler



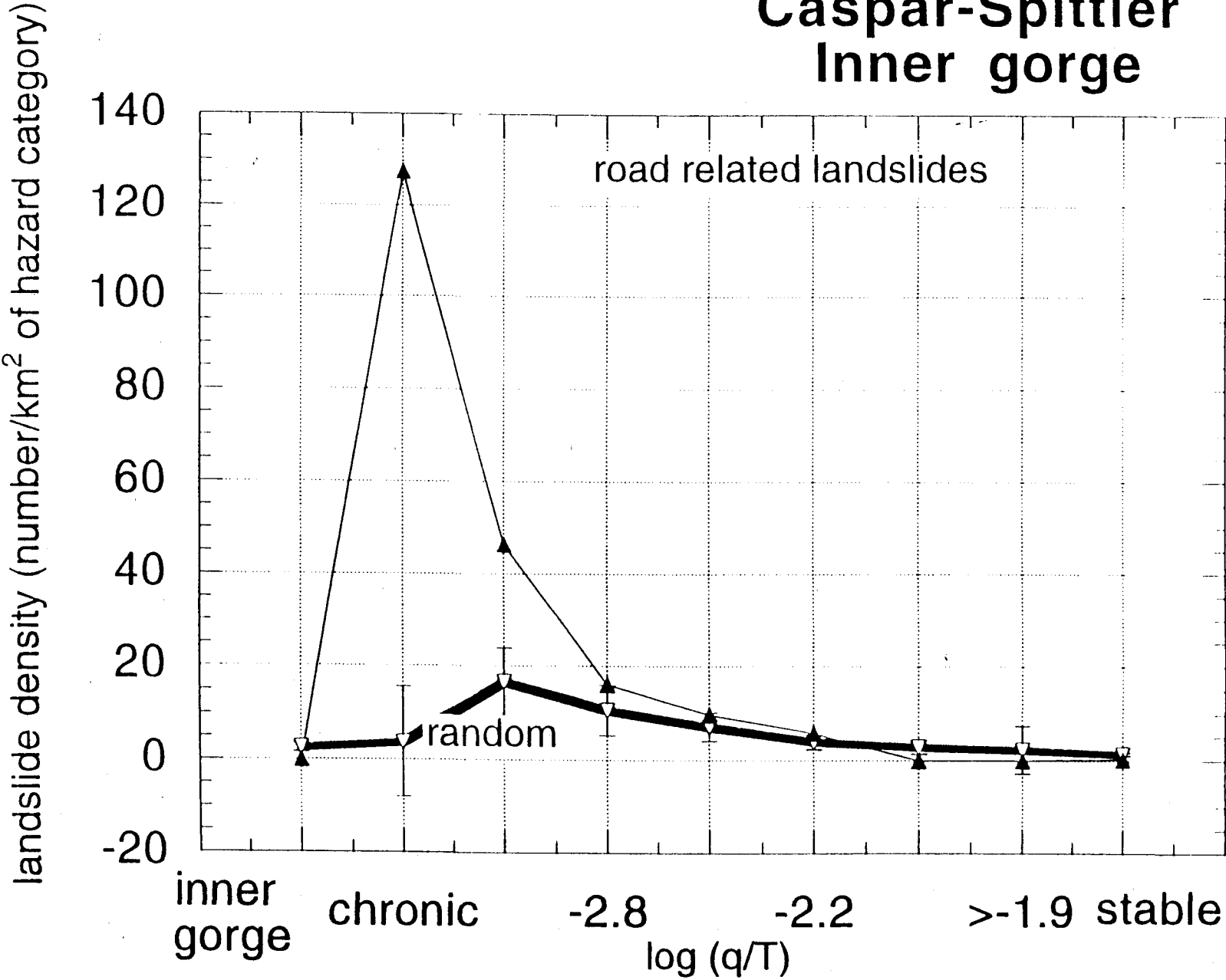
Caspar-Spittler (inner)



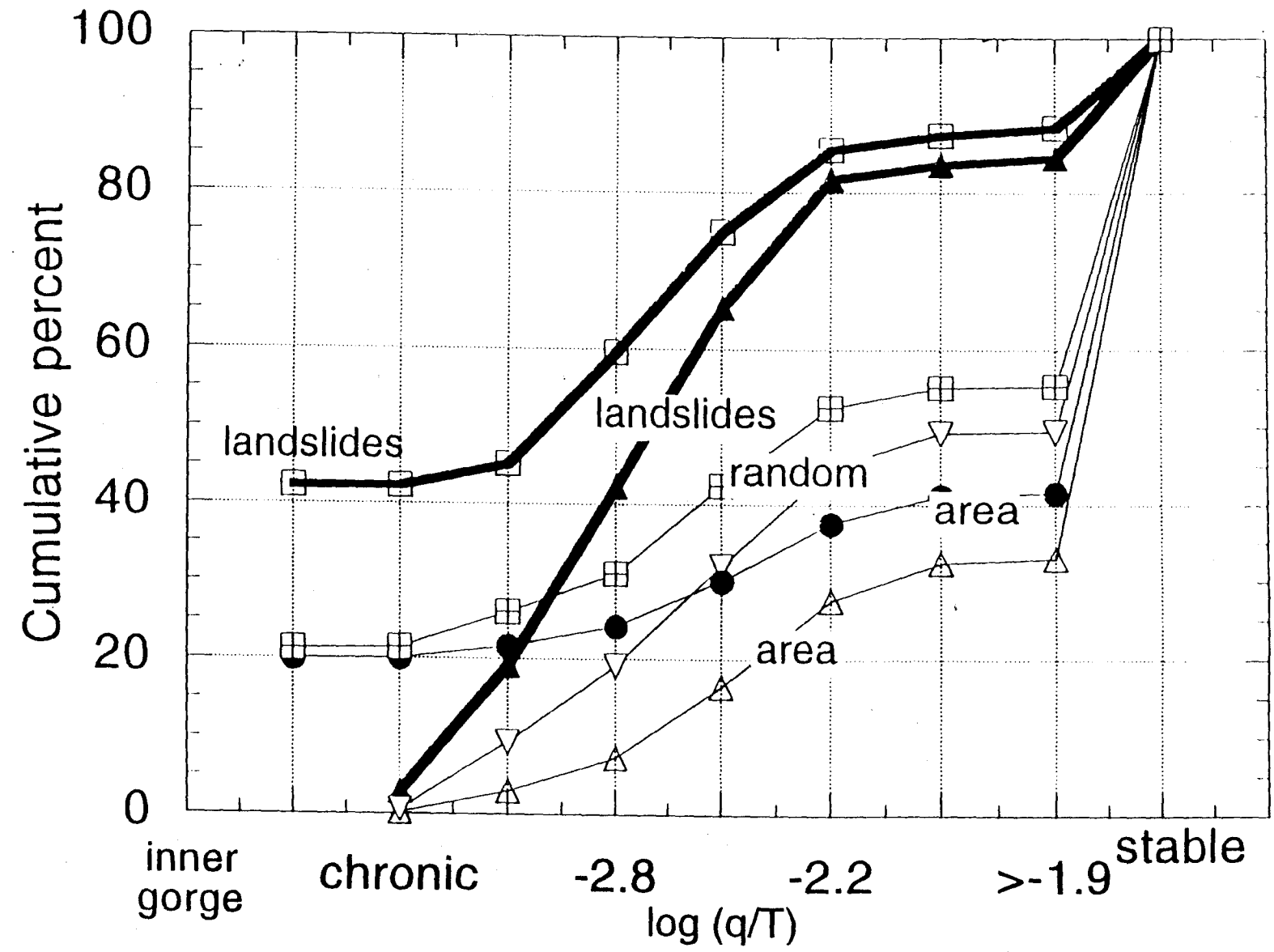
Caspar-Spittler



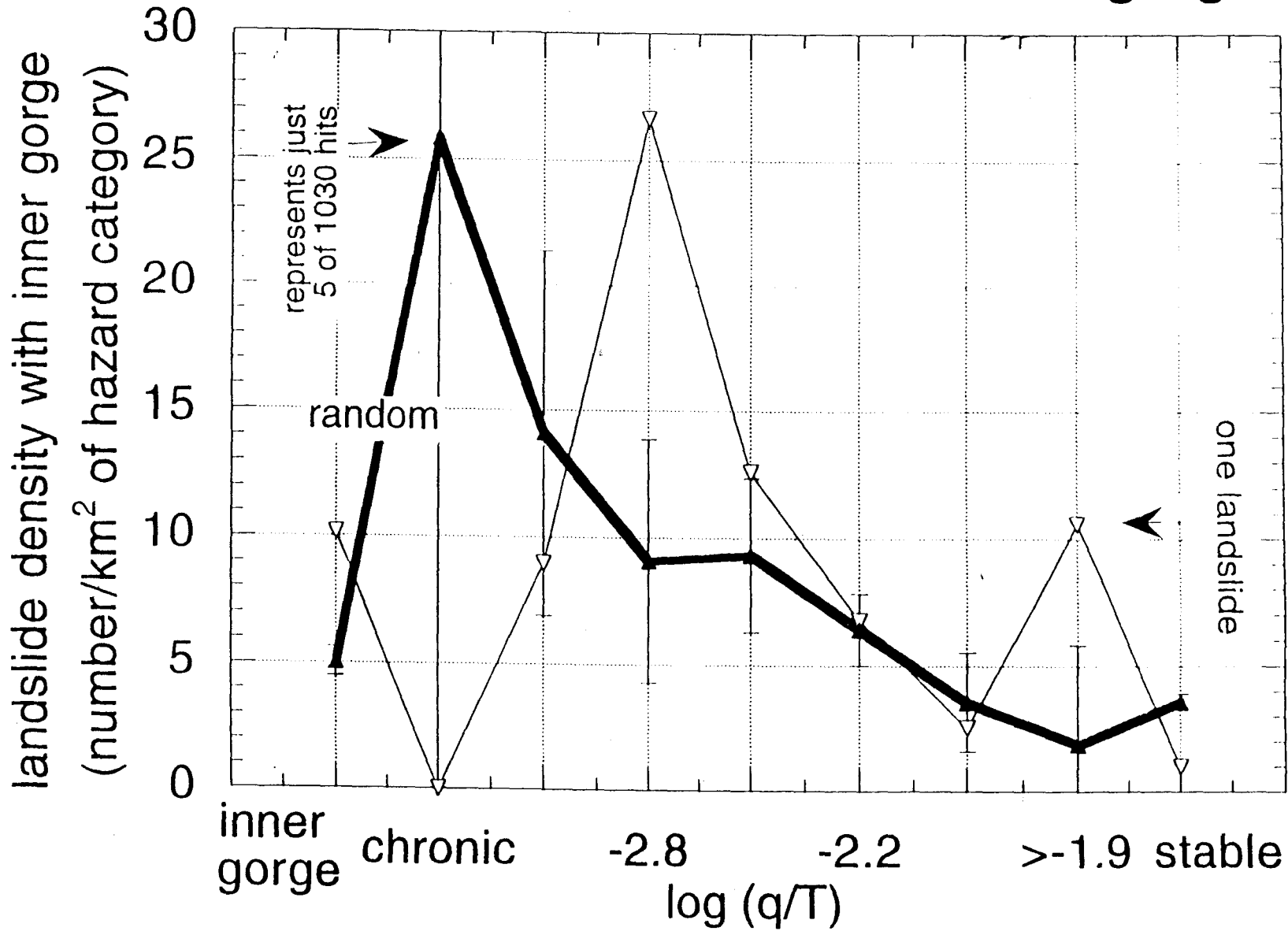
Caspar-Spittler Inner gorge



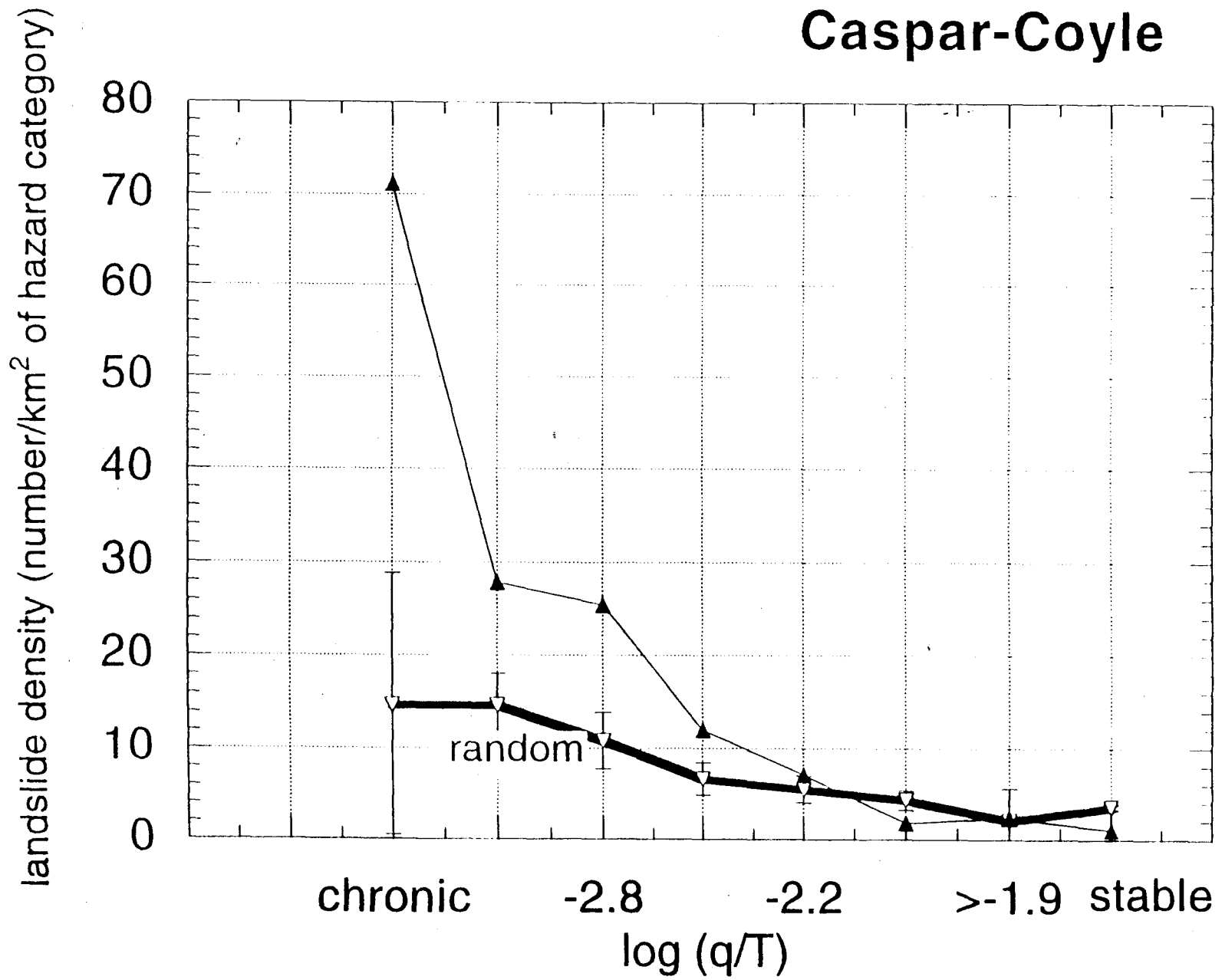
Caspar-Coyle



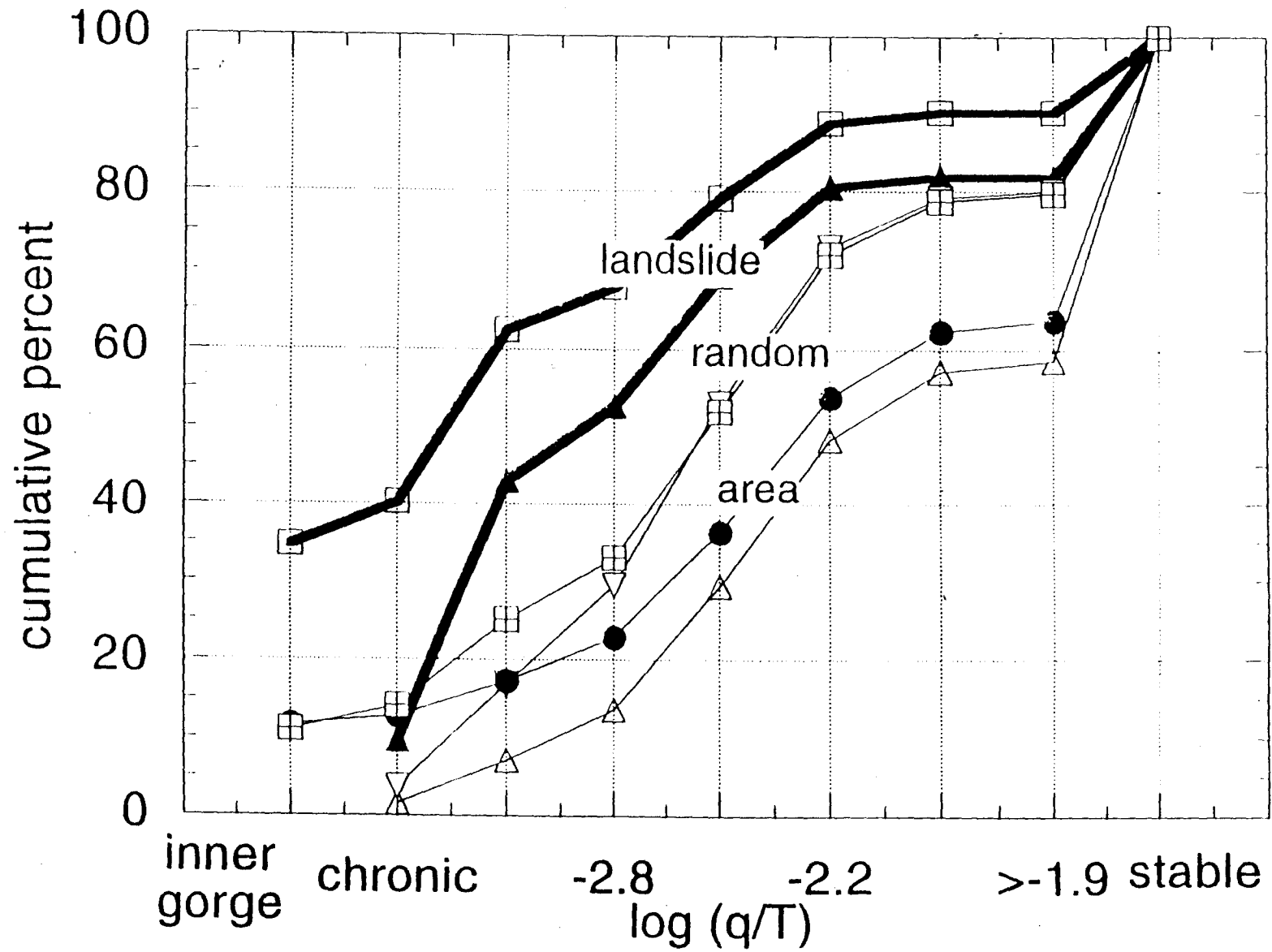
Caspar-Coyle with inner gorge



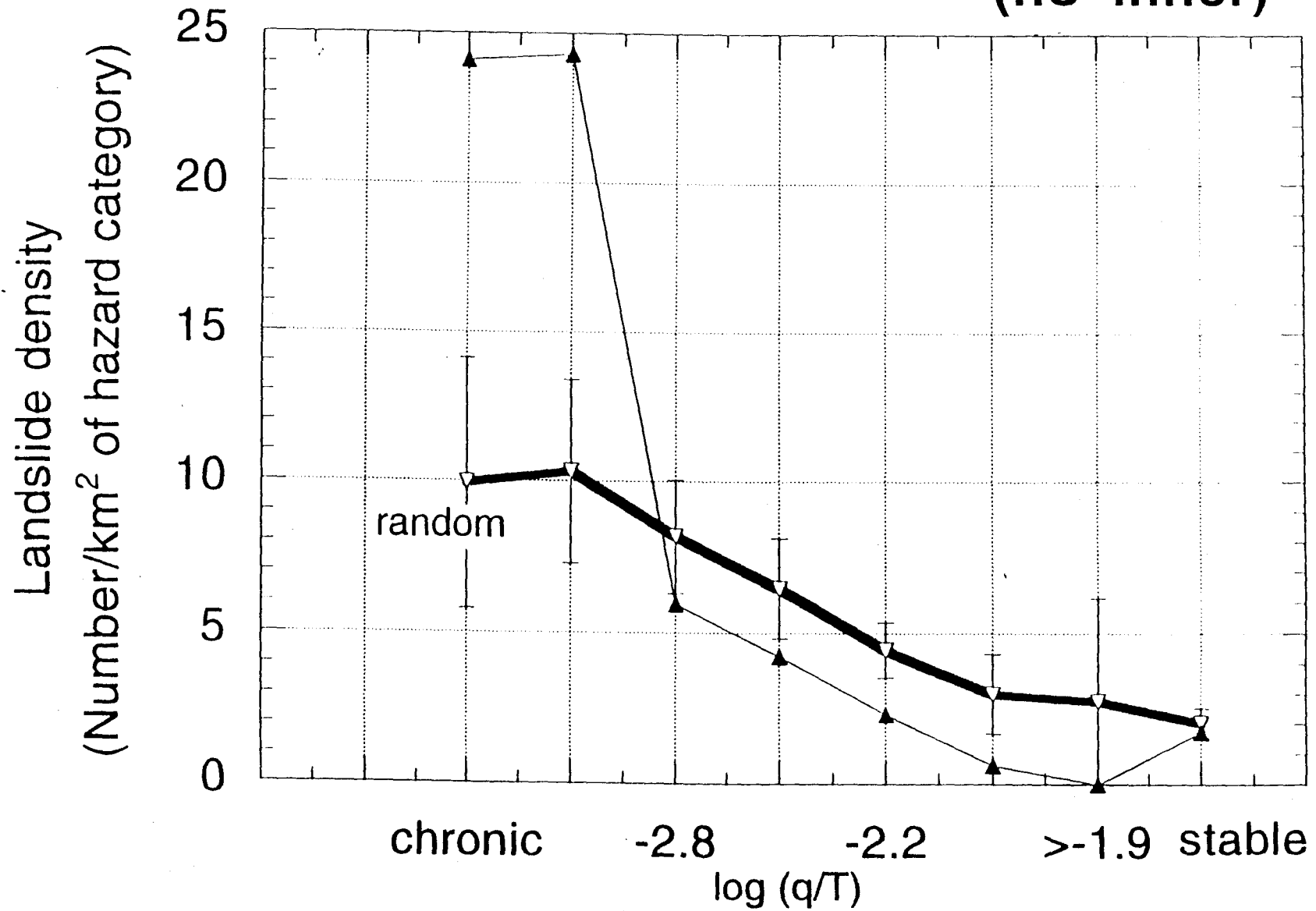
Caspar-Coyle



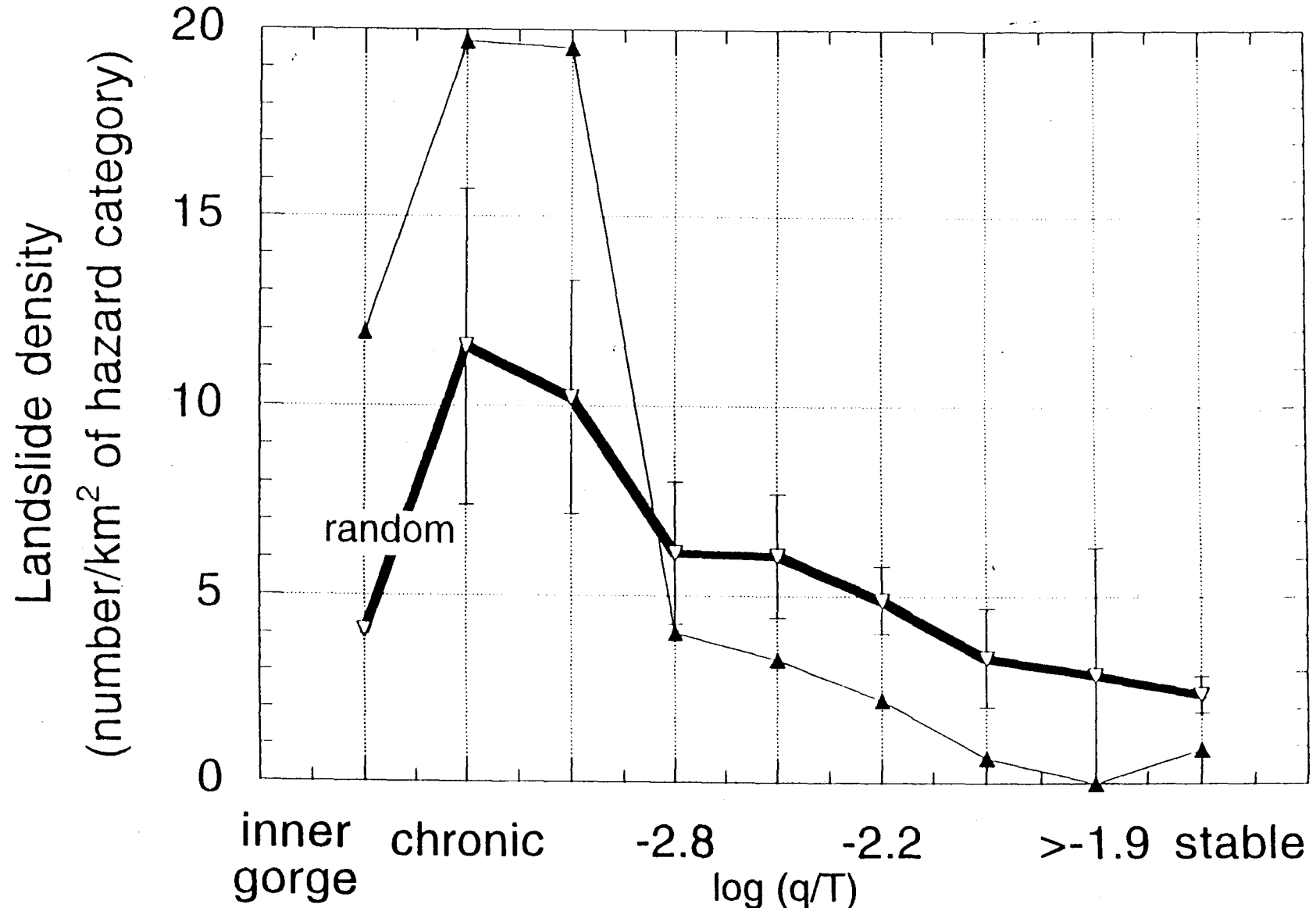
James



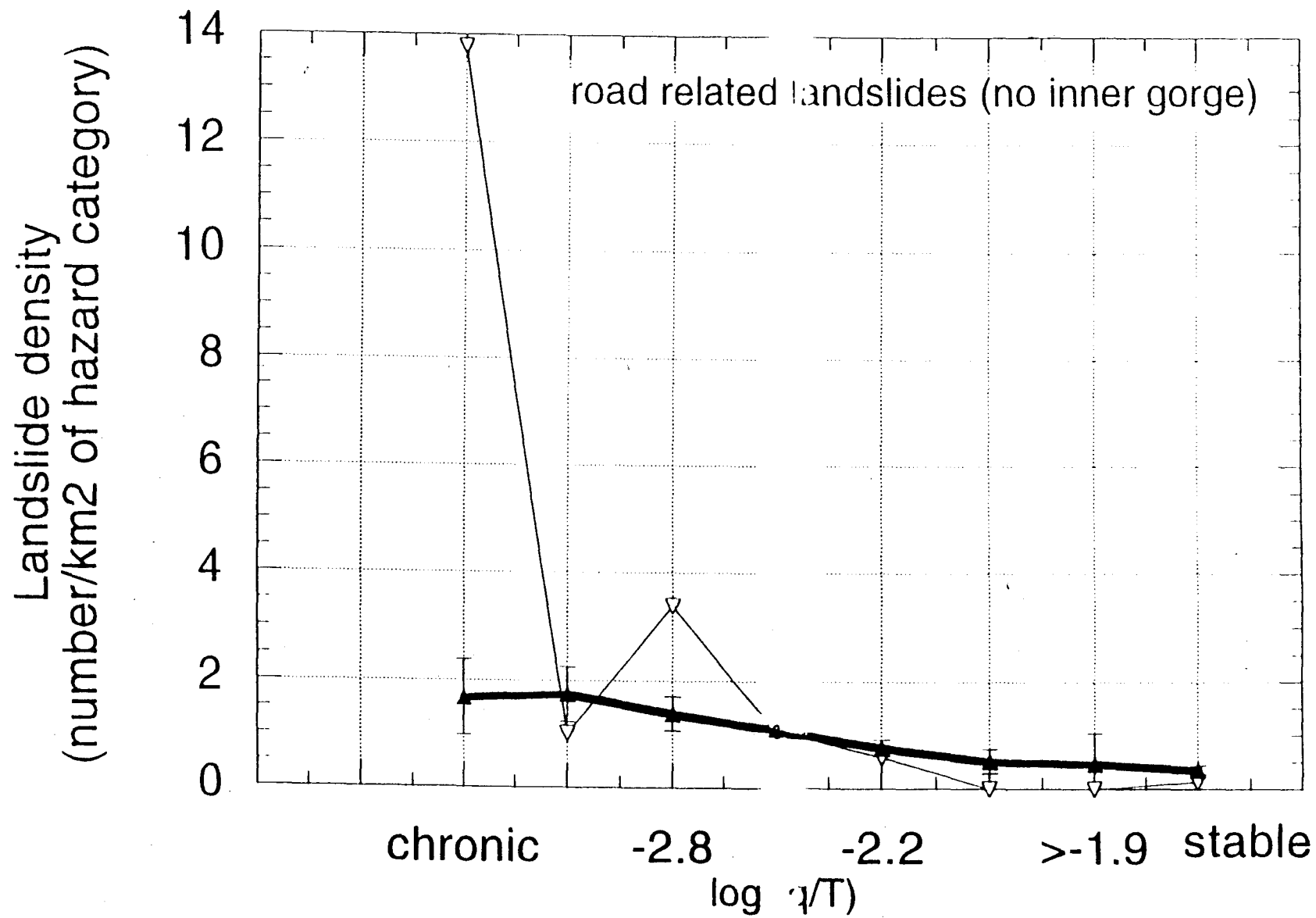
James (no inner)



James



James



**James
(inner gorge)
roads**

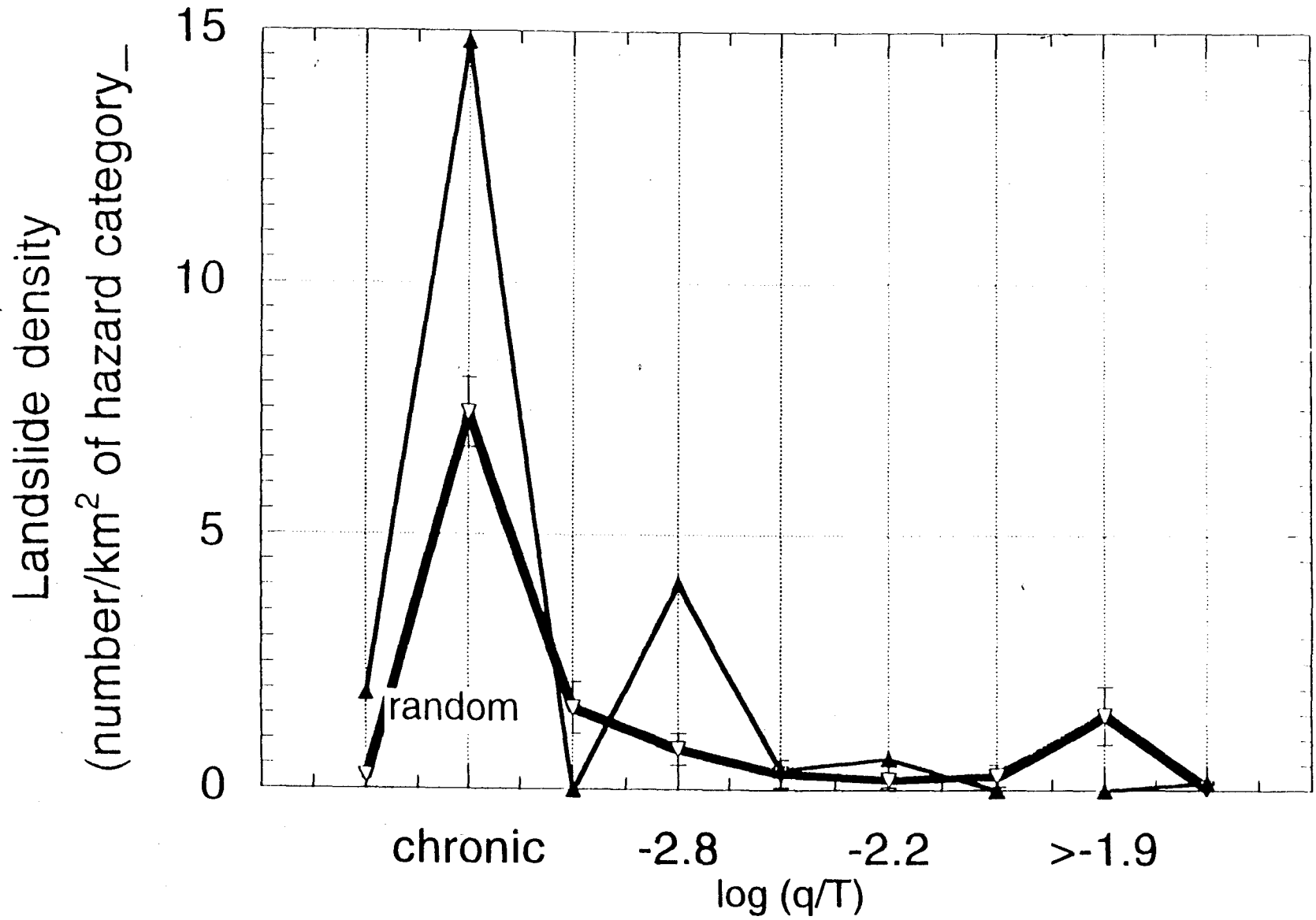


Figure 2a

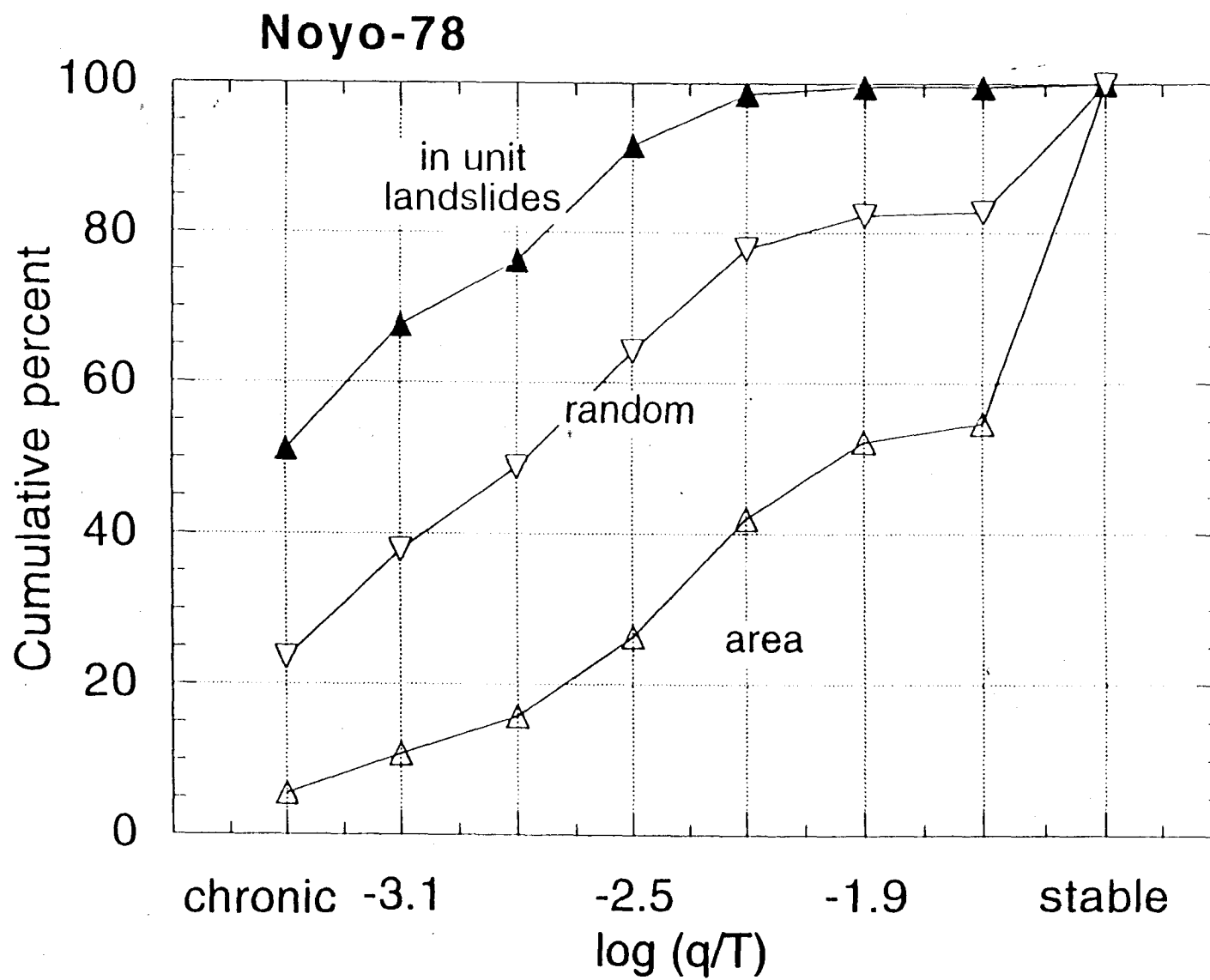


Figure 2b

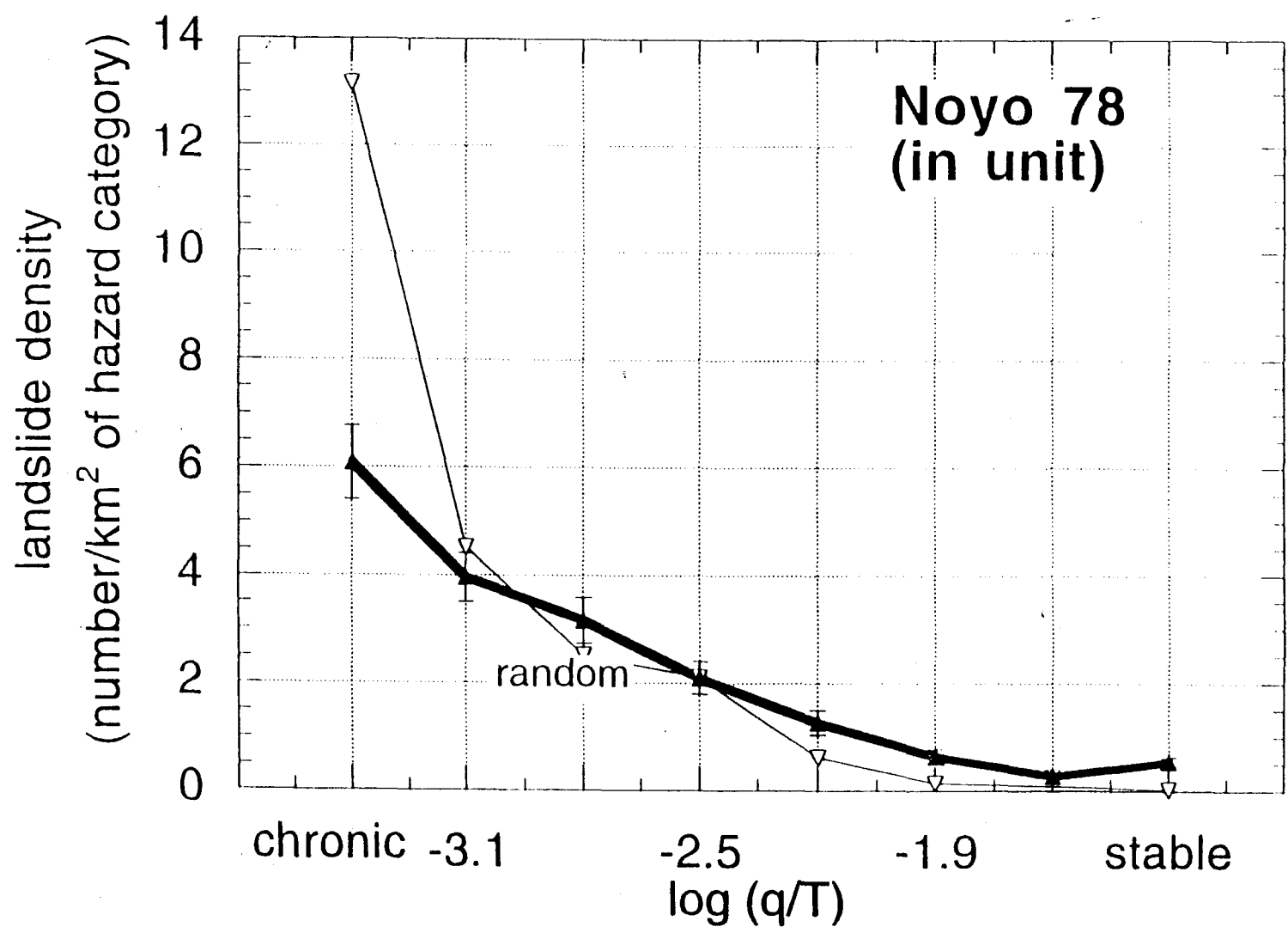
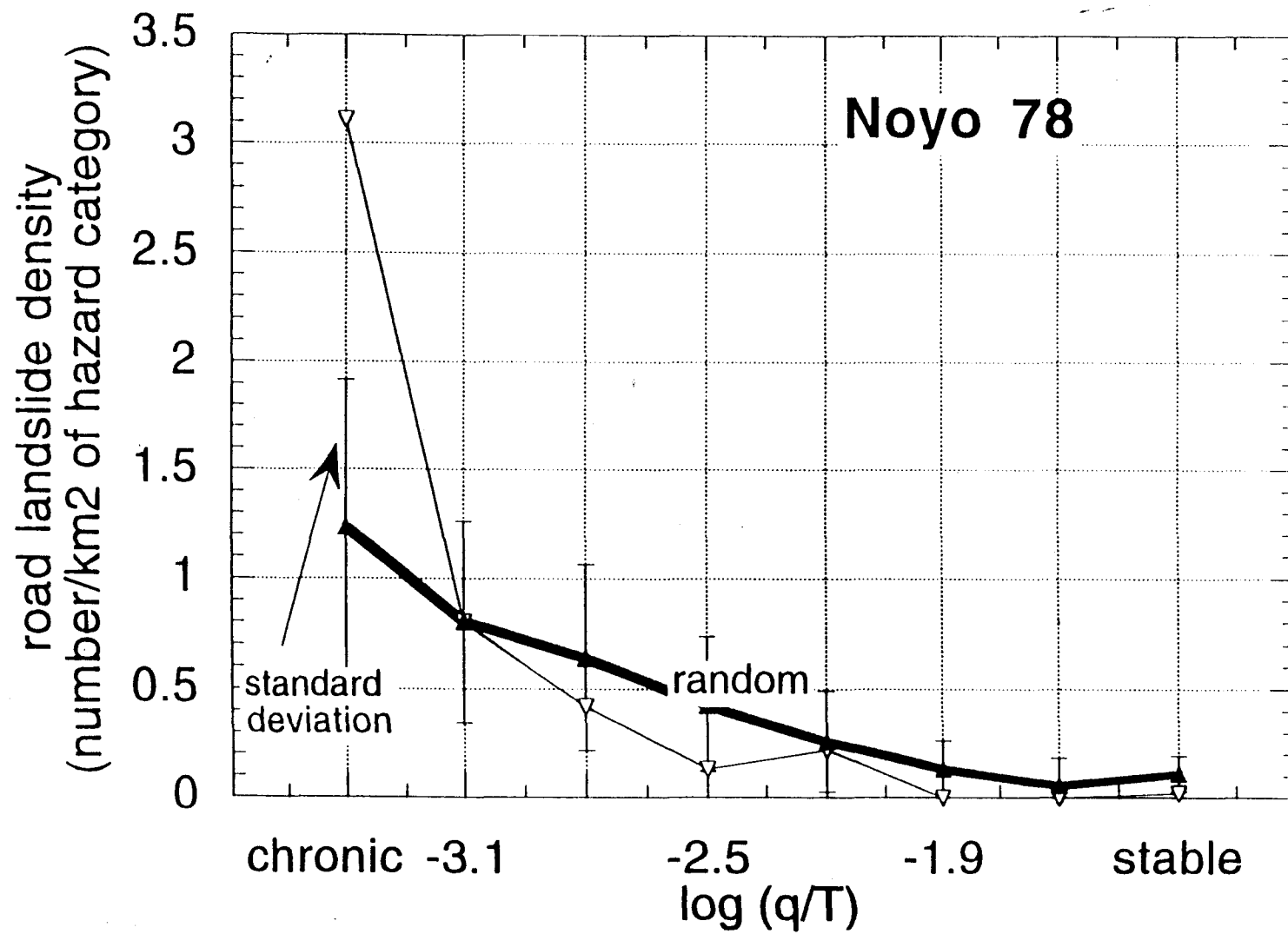
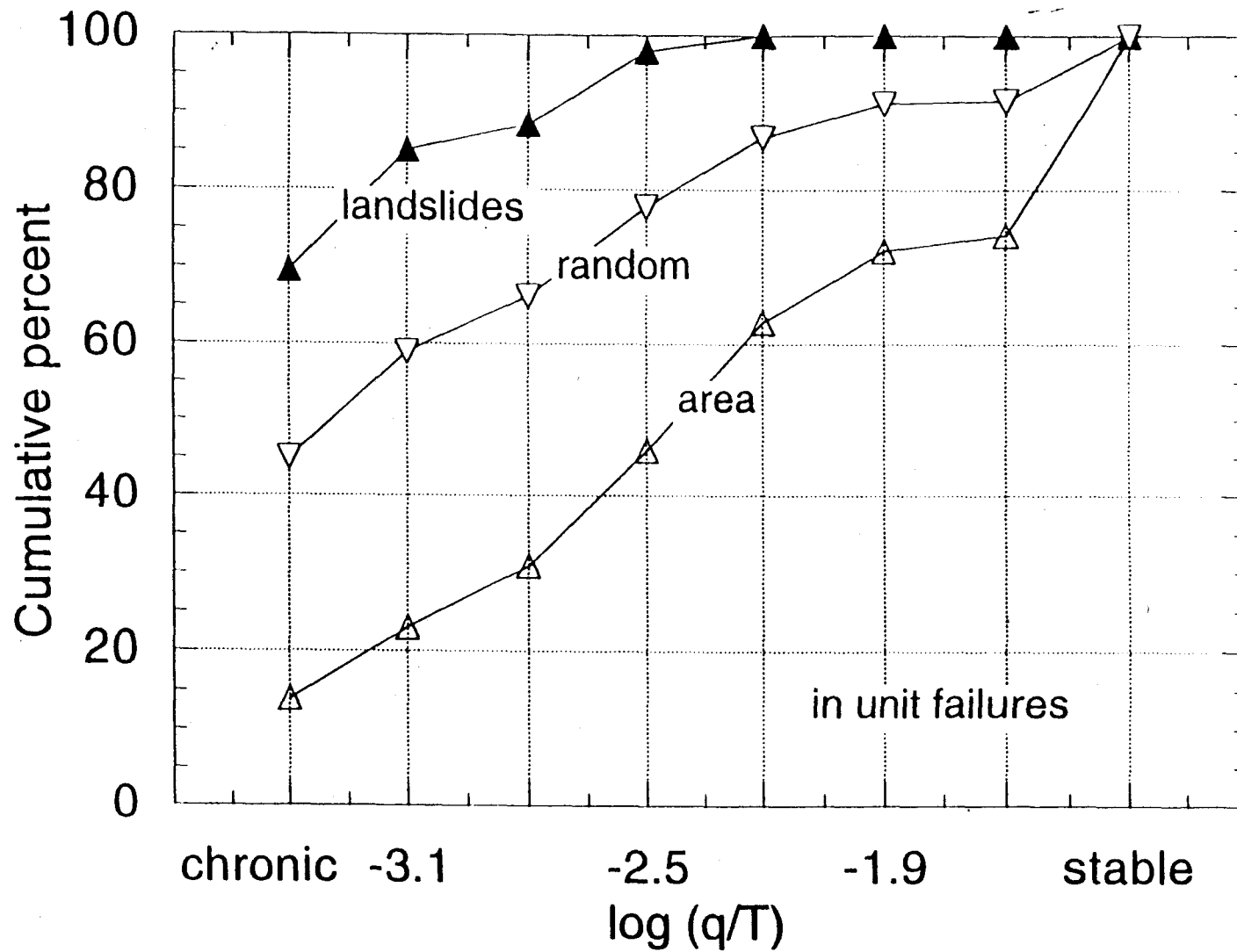


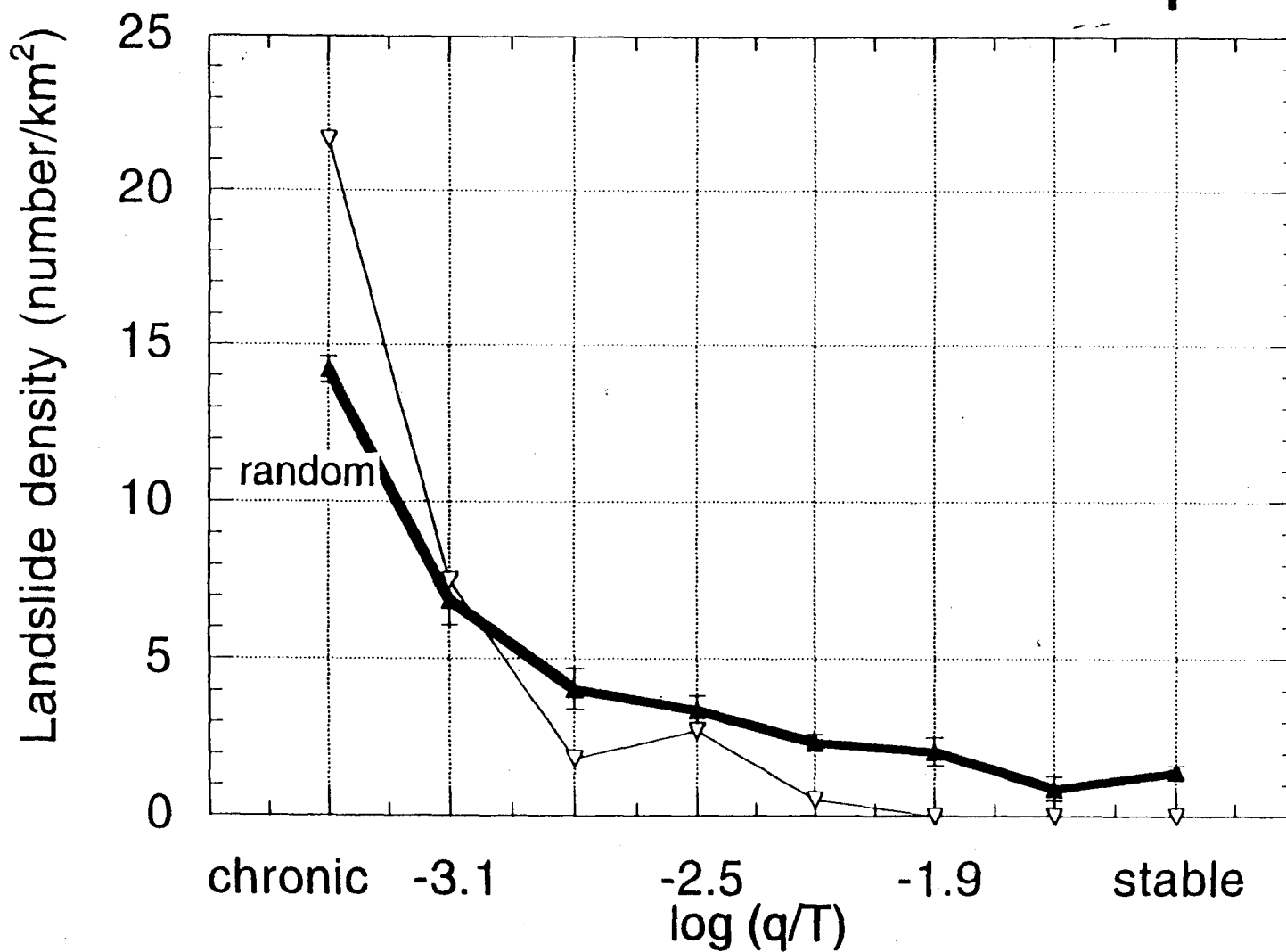
Figure 2c



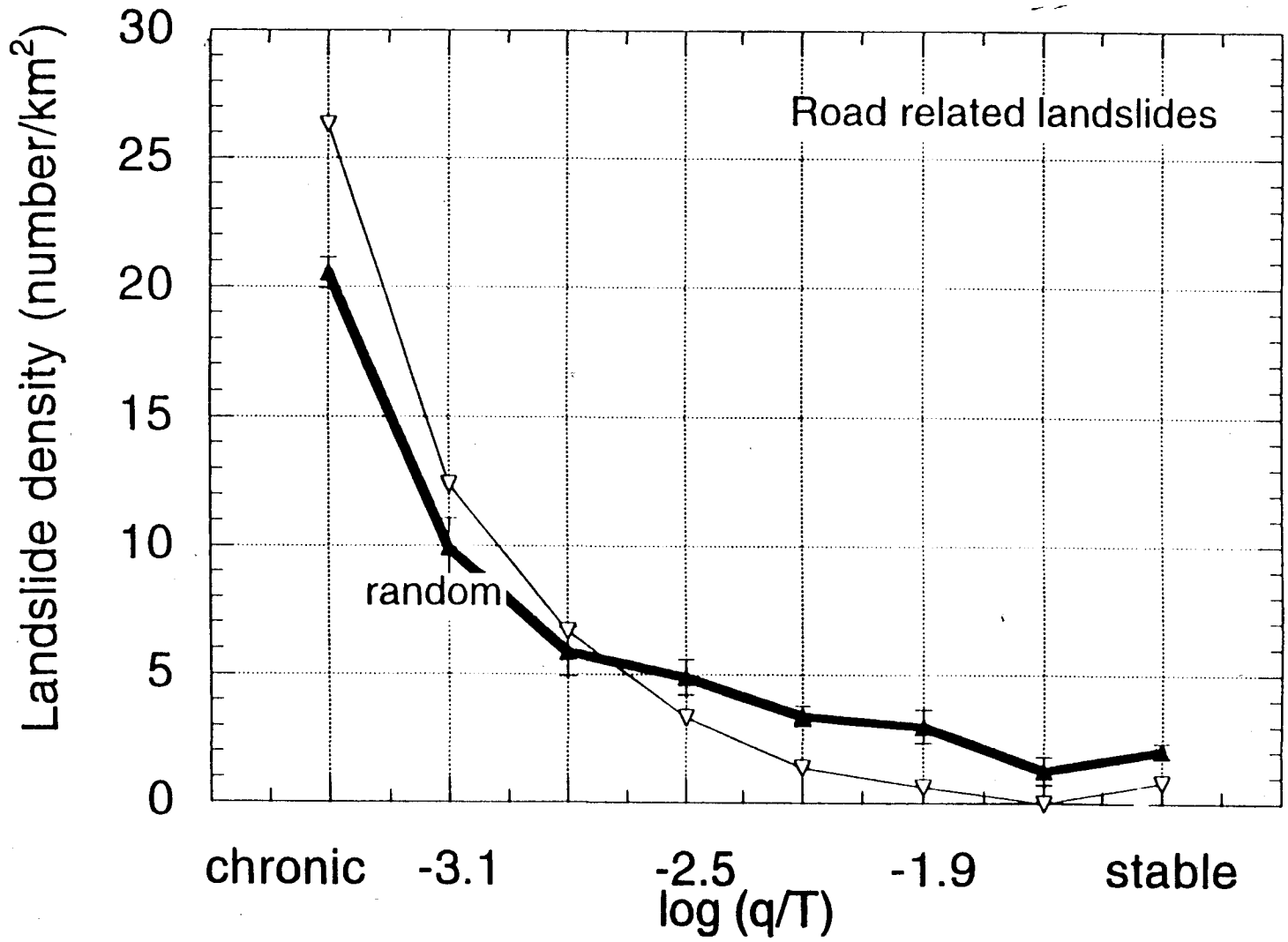
Rockport

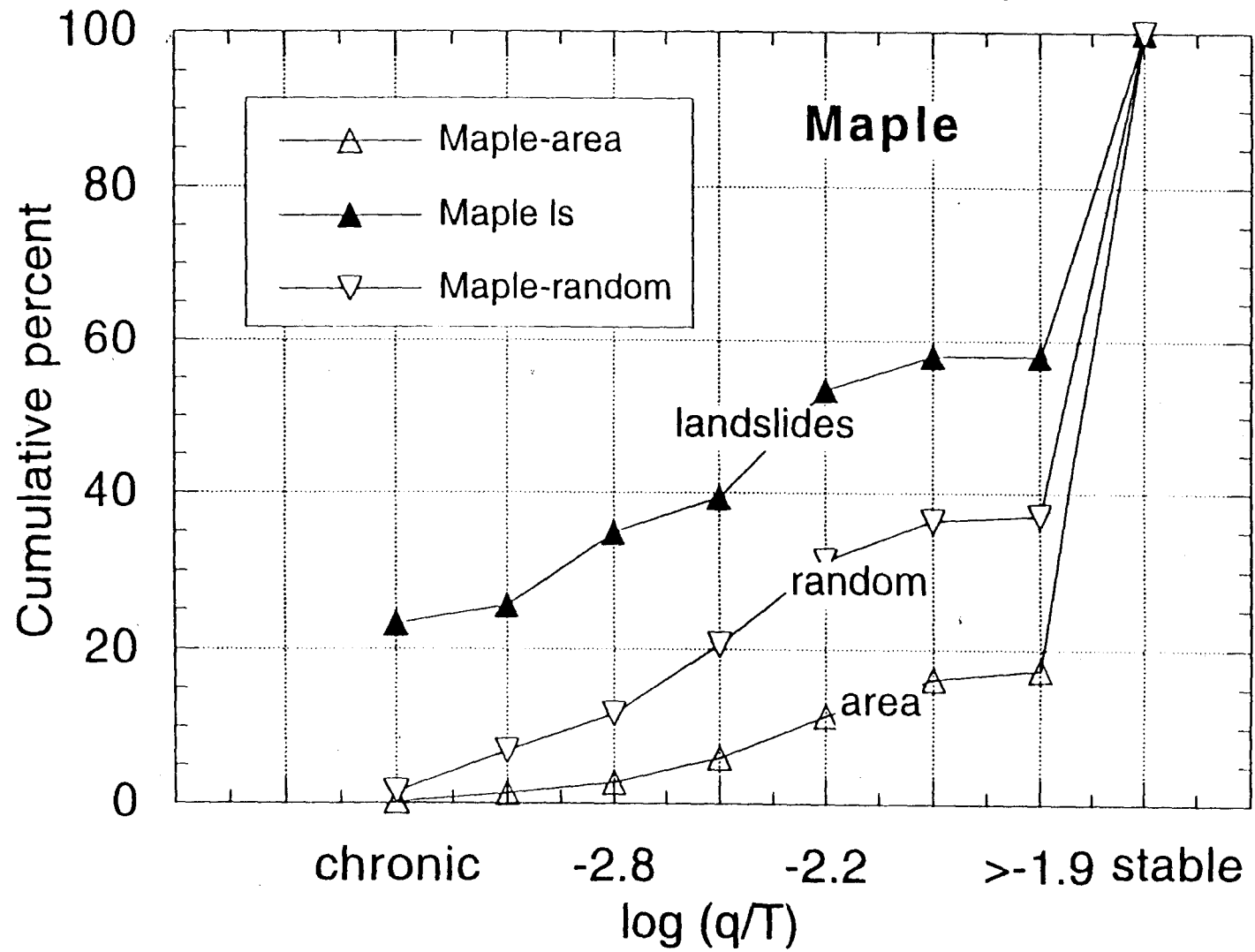


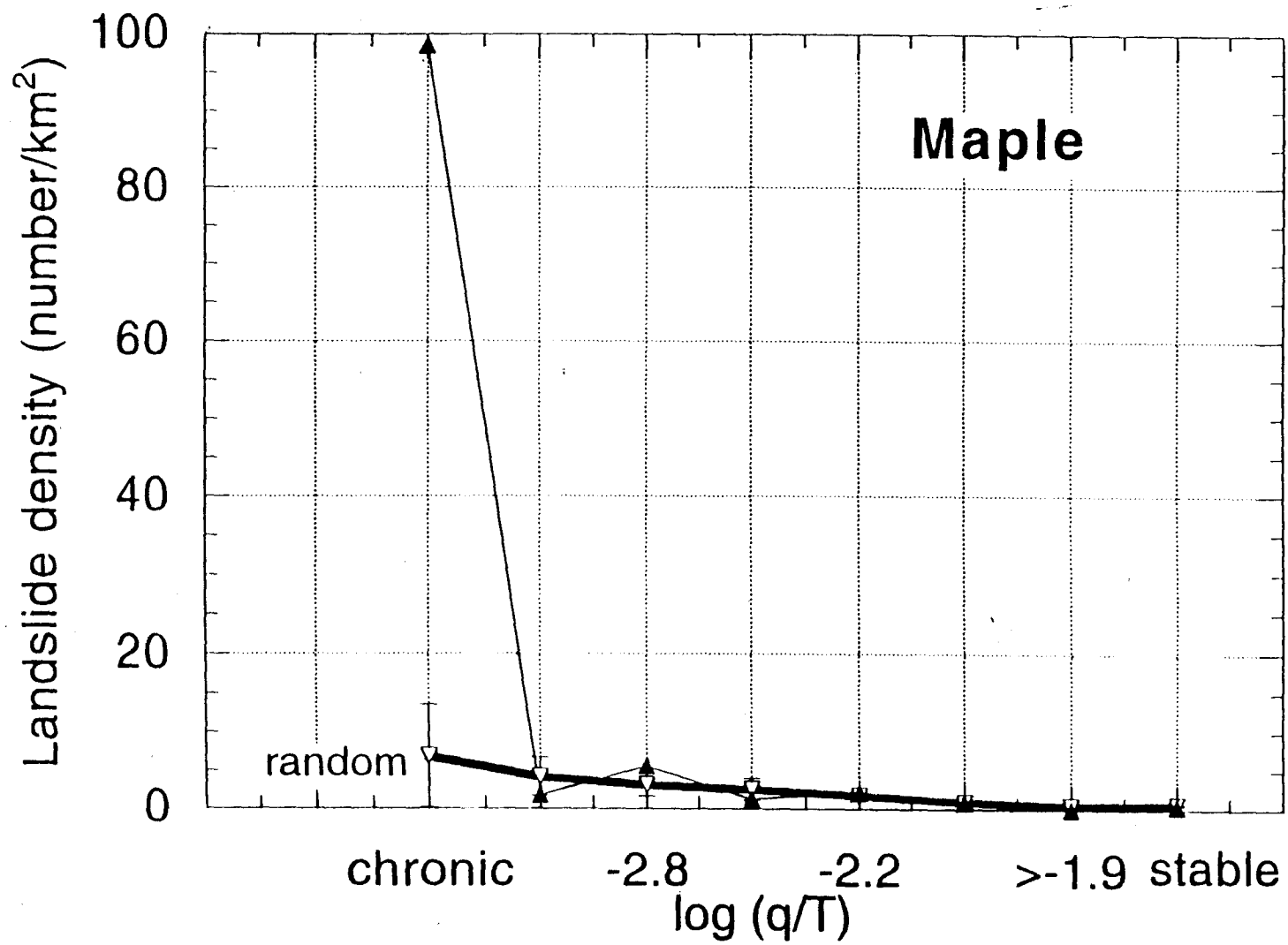
Rockport



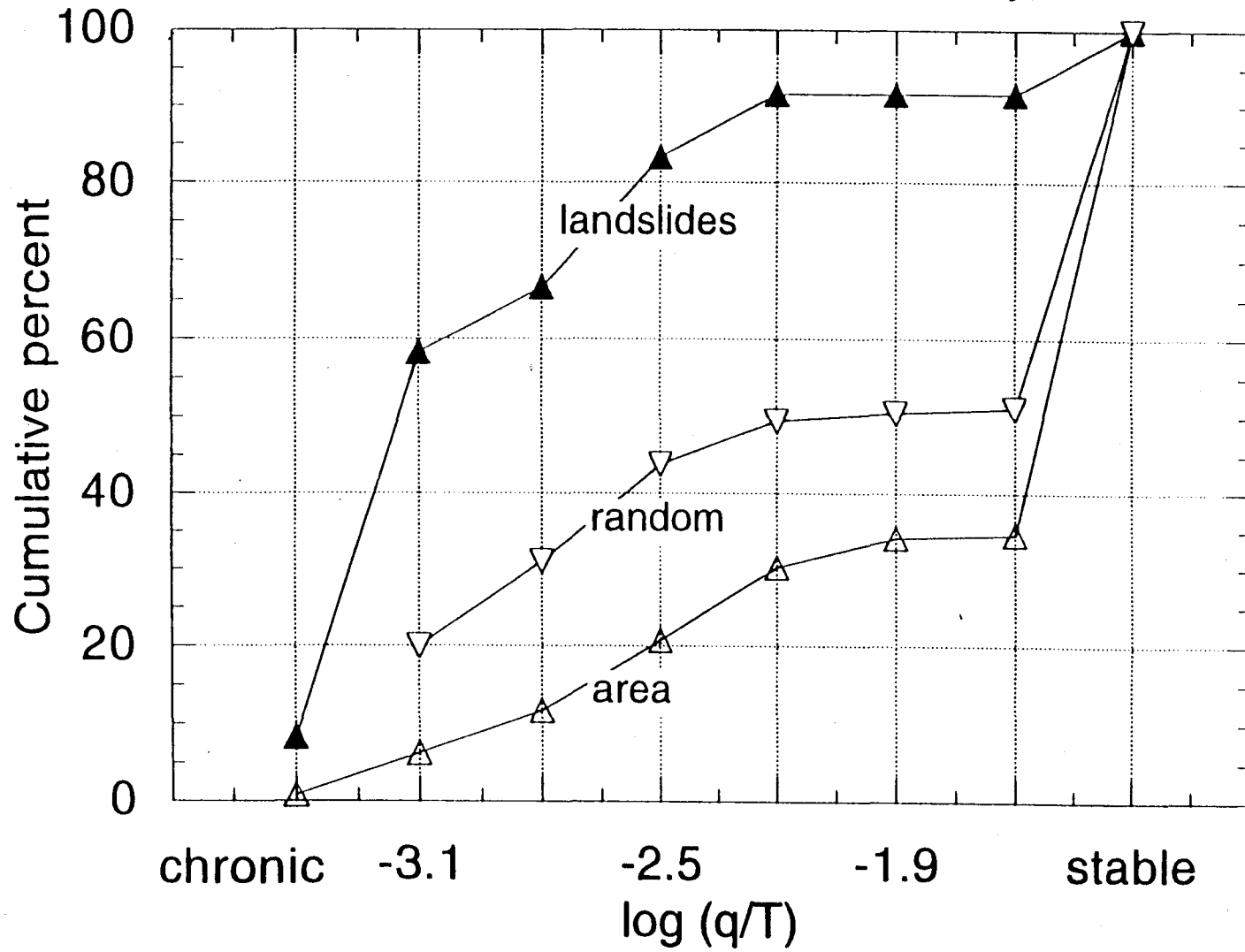
Rockport







McDonald



McDonald

